Nuclear Histone 3 Post-translational Modification Profiling in Whole Cells using Spectral Flow Cytometry

Histone H3 modification profiling using spectral flow

Carly S Golden[1*], Saylor Williams[1*], Sophia Blankevoort[2], Anna Belkina[1,3], H. Joseph Yost[4], Maria A Serrano[1‡]

[1]Center for Regenerative Medicine, Department of Medicine, Boston University Chobanian & Avedisian School of Medicine, Boston, USA

[2]John and Marcia Price College of Engineering, University of Utah

[3]Flow Cytometry Core Facility, Boston University Chobanian & Avedisian School of Medicine, Boston, USA

[4] The University of Utah, Salt Lake City, Utah and The Catholic University of America, Washington DC, USA

‡ For correspondence: maserr@bu.edu

*Contributed equally to this work

Abstract

Discerning the dynamic nature of nuclear histone 3 post-translational modifications (H3-PTMs) is crucial for understanding gene regulatory mechanisms. Although conventional nuclear H3-PTM flow cytometry protocols currently offer acceptable sensitivity, they typically involve isolating nuclei prior to running the assay, leading to significant sample loss and limited throughput. To address these challenges, we present a high-throughput nuclear H3-PTM spectral flow cytometry protocol conducted directly in whole cells. By performing fixation, permeabilization, and antibody incubations in a 96-well plate format, we eliminate the need for nuclei isolation, thereby preserving sample integrity and increasing throughput. Notably, this protocol allows for the simultaneous assessment of histone PTMs, cytoplasmic proteins, plasma membrane receptors, and cell cycle analysis within the same cell, providing comprehensive insights into the status and functional utility of a cell. This approach not only streamlines experimental procedures but also enhances the efficiency and reproducibility of nuclear flow cytometry assays, allowing for a deeper exploration of epigenetic regulation across diverse biological samples.

Summary Statement

We present a protocol for multi-parameter analysis of cell cycle, histone modifications, and caspase 3 in NPCs, utilizing spectral flow cytometry for improved sensitivity and sample integrity without nuclear enrichment.

Keywords: Spectral Flow Cytometry, Histone 3 post-translational modifications, Cell Cycle, Human induced pluripotent stem cells

Introduction

Cell cycle dynamics and histone modifications are critical in regulating lineage-specific gene expression during cell differentiation (Calder et al., 2013; Coronado et al., 2013; Hansen et al., 2008). Chromosome structure undergoes significant changes in histone modifications across various cell cycle phases during lineage commitment (Petruk et al., 2012). For instance, differentiating mitotic stem cells exhibit extended G1 phases as they exit pluripotency (Calder et al., 2013). Cell identity is established through progressive alterations in chromatin structure, driven by epigenetic mechanisms, including post-translational modifications (PTMs) of histones and lineage-specific transcription factors (Grigoryev et al., 2006; Larson and Yuan, 2012). Notably, H3 undergoes substantial PTM changes during germline induction

(Weng et al., 2012). Recent work identifies a role of H3K27ac in bookmarking stem cell identity during mitosis, preserving essential histone PTMs and transcription factors (Yiyuan Liu et al., 2017). Therefore, to effectively identify regulatory mechanisms involved in lineage establishment, it is crucial to apply methods that can capture the dynamic changes in histone PTMs while resolving different cell cycle phases and cell identity marks.

Histone profiling via flow cytometry enables the study of global histone modification changes, providing detailed insights into chromatin dynamics at the single-cell level (Bergamasco et al., 2024; Ronzoni et al., 2005). However, traditional methods require isolating live cell nuclei and staining them in round-bottom tubes, which can lead to sample loss. Additionally, conventional flow cytometry uses a single detector per fluorophore, thus capturing only part of the emission spectrum, limiting multiplexing capabilities.

To overcome these limitations, we developed EpiFlow, an optimized whole-cell histone profiling protocol for spectral flow cytometry. EpiFlow utilizes a 96-well plate format for cell fixation, permeabilization, and staining, reducing reagent consumption and increasing throughput. Unlike most traditional histone PTM cytometry methods, our protocol does not require nuclear isolation, minimizing sample loss and enabling the detection of membrane-bound, cytoplasmic, and nuclear antigens. EpiFlow also leverages the multiplexing capability of spectral flow cytometry to increase the sensitivity of histone profiling while simultaneously collecting information from several cellular compartments and biological processes. Here, we present a validated spectral flow cytometry panel that identifies five histone PTMs typically associated with open chromatin alongside markers for cell cycle, apoptosis, and cell type identification in human induced pluripotent stem cells (hiPSC)-derived neuronal progenitor cells (NPC). To support the application, reproducibility, and improvement of EpiFlow and its analysis workflow, we created a GitHub repository (Golden et al., 2024; Lab, 2024) containing data and bioinformatic code written in a reproducible R environment (Ushey and Wickham, 2024a, 2024b), ensuring accessible and reproducible data analysis.

EpiFlow allows the assessment of several histone PTM and can resolve subtle changes across cell types and cell cycle phases in fixed samples. It offers higher resolution to explore relationships between histone PTMs, cell identity, and function, thus providing a useful tool to address complex biological questions. We propose that EpiFlow could inform, complement, and validate available next-generation sequencing approaches that examine chromatin biology.

Results and Discussion

Spectral flow cytometry employs more sensitive detectors that capture the full emission spectrum of each fluorochrome, permitting the use of larger panels to evaluate broader cell profiles (Ferrer-Font et al., 2021). Unique spectral signatures of each fluorochrome are identified through advanced unmixing techniques, addressing the compensation limitations observed in traditional flow (Novo, 2022). However, the limited availability of conjugated and validated monoclonal antibodies for histone PTMs represents a challenge for multiparametric panel design. To address this limitation during the design and validation of

98 the EpiFlow panel, we selected histone PTM antibodies that met the following criteria: (a) availability of
99 monoclonal antibodies conjugated with fluorochromes that have compatible spectral signatures for
100 multiplexing, (b) histone marks with published literature supporting their association with transcriptional
101 activation and distinct cell cycle phases; H3K27ac (Yin Liu et al., 2017; Yiyuan Liu et al., 2017), H3K4me3
102 (Lauberth et al., 2013), H3K9ac (Krejčí et al., 2009), H3K14ac (Kueh et al., 2023), H3K14ac+pH3 (Lo et
103 al., 2000), H3K9ac+H3K14ac (Armenta-Castro et al., 2020; Karmodiya et al., 2012; Liu et al., 2023) and,
104 (c) known response to small molecules that will increase or decrease histone mark levels for validation
105 purposes. This resulted in an initial histone H3 PTM core panel for H3K9ac, H3K14ac, H3K4me1, H3K4me3
106 and H3K27ac. Additional features to identify live/dead cells, total H3, distinct cell types, mitotic cells,
107 apoptotic cells, and to resolve cell cycle phases were added based on spectral compatibility with the core
108 H3-PTM panel (Supplementary Table 1). Our staining protocol was optimized to measure nuclear histone
109 PTMs and features of interest across subcellular compartments in fixed whole cells. However, a significant
110 challenge of this multiplexing approach is to preserve the integrity of membrane-bound epitopes while
111 ensuring optimal fixation and permeabilization for proper access of antibodies to the nuclear compartment
112 and antigen recognition. To validate our staining protocol for cell membrane integrity and nuclear antigens
113 accessibility, we performed immunofluorescence followed by confocal imaging of SCTi-003A hiPSCs
114 stained with H3K9ac and beta-catenin (a membrane marker) (Fig. S1).

115 To assess the specificity of the selected antibodies, we treated SCTi-003A hiPSC and WTC11 hiPSC-
116 derived NPCs and with Trichostatin-A (TSA), SAHA (Vorinostat), or A-485 to modulate histone H3
117 acetylation levels (Lasko et al., 2017; Richon et al., 1996; Seuter et al., 2013). TSA and SAHA are histone
118 deacetylase I/II (HDAC) inhibitors that increase histone acetylation, while A485 is a histone
119 acetyltransferase (HAT) inhibitor targeting p300/CBP, which reduces histone acetylation. We evaluated
120 EpiFlow sensitivity using three different concentrations of these selective inhibitors and tested whether we
121 could detect subtle changes in H3-PTMs across cell cycle phases. Our experiments in hiPSCs and NPCs
122 showed a significant and dose-dependent change, either increasing (TSA and SAHA) or decreasing (A-
123 485) median fluorescent intensity values (MFI) of H3K27ac, H3K4ac, and H3K9ac marks (Fig. S2, S3). Our
124 results also showed distinct changes in the distribution of fluorescence intensity values of each H3-PTM
125 depending on the expression levels of PAX6 (NPC marker) and whether cells were on G0/G1, G2, or mitosis
126 (Fig. S2 D, E). MFI is one of the most common statistics used to measure the shift in fluorescence intensity
127 of a cell population. However, MFI values report the central tendency of a cell population and do not provide
128 information about the distribution of the expression for a feature of interest (Herzenberg et al., 2006;
129 Roederer et al., 2004). This is particularly relevant for experimental designs that aim to identify subtle
130 changes in the features tested, such as histone H3 acetylation and methylation levels, as a response to
131 drug treatments. TSA and A-485 are highly specific HDAC and HAT inhibitors, respectively, widely used to
132 assess changes in histone H3 acetylation (Lasko et al., 2017; Vigushin et al., 2001). Therefore, we
133 proposed that TSA and A-485 treatments would not change the fluorescence intensity values of histone H3
134 methylation marks (H3K4me), further validating EpiFlow specificity. Interestingly, H3K4me1 fluorescent

intensity (FI) values showed significant differences between treatments and across cell cycle phases (Krustal-Wallis test G0/G1 $\chi^2(6) = 4380.63$, $p<0.0001$; G2 $\chi^2(6) = 817.47$, $p<0.0001$; Mitosis $\chi^2(6) = 236.45$, $p<0.0001$, Supplementary GitHub analysis, Methods Validation section). Our analysis also showed that H3K4me1 MFI varied with treatment and cell cycle phase, with the TSA group showing an overall more pronounced effect than A-485, particularly in mitosis. However, in all treatment groups, H3K4me1 MFI values shifted in the same direction towards higher intensity values without affecting their distribution (Supplementary GitHub analysis, Methods Validation section). The observed H3K4me1 changes could indicate a technical limitation of our approach or suggest an alternative hypothesis in which modulation of H3 acetylation might also influence H3K4 methylation levels (Bui et al., 2010; Crump et al., 2011; Lee et al., 2006). This prompted us to validate the sensitivity of our panel with two independent approaches that used conventional flow cytometry to measure histone H3K4 methylation levels in hiPSCs treated with either OICR-9429 or CPI-455 HCl and in an hiPSC line with a homozygous loss of function (LOF) mutation in the histone methyltransferase gene *KMT2D* (KMT2D10.4). The small molecule OICR-9429 is a potent antagonist that inhibits the WDR5-MLL complex responsible for mediating H3K4me3, consequently reducing this mark (Grebien et al., 2015). CPI-455 HCL selectively inhibits the lysine demethylase KDM5, leading to an increase in global levels of H3K4me3 (Vinogradova et al., 2016). The *KMT2D* LOF hiPSC cell line was generated using a CRISPR/Cas9-targeted 2 base pair deletion in exon 2 of *KMT2D* gene in a WTC11 hiPSC line (File S1). This line is expected to exhibit reduced levels of H3K4 methylation compared with its isogenic control. WTC11 hiPSCs treated with OICR-9429 and CPI-455 HCL showed the expected shift in the magnitude and direction of H3K4me3 MFI (Fig. S4 A). This was further supported by a significant reduction of H3K4me2 and H3K4me3 MFI values in the *KMT2D* LOF iPSC line compared with its isogenic control (Fig. S4 B). Notoriously, H3K4me1 levels were equivalent in *KMT2D* LOF and WTC11 hiPSC lines, which aligns with recent studies reporting redundant H3K4me1 activity by other KMT2 methyl transferases in mouse embryonic stem cells (Kubo et al., 2024). Our data, generated from three different hiPSC lines (SCTi-003A, WTC11, and KMT2D10.4), in two cell types (hiPSC and NPC), acquired across two instruments (Aurora Cytek and Stratedigm S1000EXi) demonstrate that EpiFlow can detect histone H3 PTMs with high sensitivity and specificity. Additionally, our analysis underscores the importance of resolving the cell cycle status of cell populations to identify histone PTM changes accurately.

The simultaneous assessment of several cellular parameters in one experiment allows high-resolution profiling of complex samples, rare cell populations, or highly dynamic biological processes in specific cell lineages. We hypothesized that EpiFlow could resolve distinct alterations of histone H3 PTM across cell cycle phases in a single cell lineage, and that subtle variations in these modifications would contribute to subcluster formation within each cell cycle phase. We again applied the core EpiFlow panel (H3K4me3, H3K9ac, H3K27ac, H3K14ac and H3S10ph) to hiPSC-derived NPCs and included features that identify live cells (Live/Dead staining), apoptotic cells (Cleaved-Caspase3), NPC (PAX6) and cell cycle phases (FxCycle) (Protocol S1, Table S1). All experiments were performed in triplicates (defined as one hiPSC line cultured in three different wells followed by NPC induction) and included unstained cells and single-color

172 controls (SCCs) using beads or cells. After acquisition and unmixing (Details in Protocol S1, Supplementary
173 File 2 and Analysis Note section in main manuscript), data was pre-processed following field standards to
174 remove low-quality events (Fig. 1, A-D) and enhance signal sensitivity and specificity (Supplementary File
175 3) (den Braanker et al., 2021; Herzenberg et al., 2006; Park et al., 2020). We used a traditional two-
176 dimensional gating strategy as a benchmark for a more exhaustive, unsupervised assessment and
177 exploratory analysis (Fig. 1 E-L). While downstream analysis used unsupervised algorithms, we defined
178 the minimum expected cluster resolution to inform parameter selection and workflow. The criteria for
179 minimum expected clusters considered a relatively homogeneous cell population (NPC with varying
180 degrees of PAX6 expression) captured at one of three possible stages of the cell cycle (based on markers
181 used, G0/G1, G2, or Mitosis (M)) or undergoing apoptosis (Cleaved-Caspase3) and that should have subtle

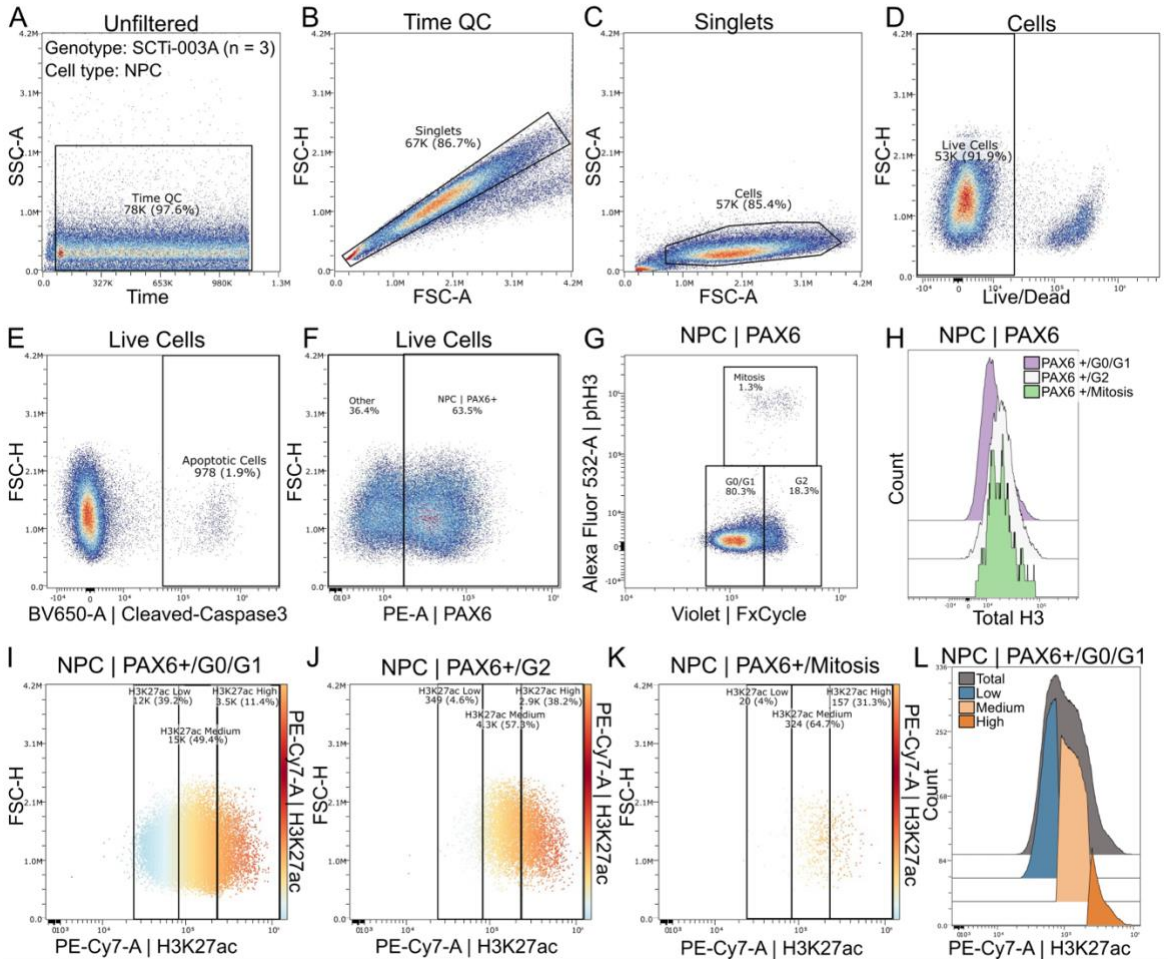

Figure 1. Scatter plots and histograms showing manual gating strategies to select high quality events and to identify neuronal progenitor cells, their cell cycle status, and histone H3-PTM fluorescence values. (A-D)**.** Cell quality gates to capture single cells recorded at a stable flow rate during acquisition. Subsampling and downstream analyses were performed using Live Cells gate. (E-L) Traditional two-dimensional gating strategy. (E) Within the live cells group, late apoptotic cells (cleaved-Caspase3 positive) are identified. (F) NPCs (PAX6 positive cells) were gated to include cells with low PAX6 expression levels ("Other"). (G) FxCycle and H3S10ph (pH3-S10) gates were used to identify NPCs in G0/G1, G2, and mitosis. (H) Histogram showing levels of total H3 at G0/G1, G2, and mitosis. Note comparable levels of total H3 during G2 and mitosis. (I-L) Gates to identify low, medium, and high fluorescence intensity values of H3K27ac in each cell cycle phase. Color-scale in panels I-K is used to aid more precise gating of H3 PTM features expected to be distributed as gradients rather than positive-negative cell populations. The same gating strategy was applied to all other H3-PTM assessed. Percent values (%) represent the events of a given gate present in root gate Live cells. A color scale bar on the right side of plots (I-K) represents the feature fluorescence intensity range to allow precise gating.

182 differences in the levels of H3 PTM. Unlike traditional single-cell transcriptional data analysis, unsupervised
183 clustering of spectral flow data is performed in high-dimensional space, followed by visualization in two-
184 dimensional space. This approach optimizes the high-dimensional data captured by EpiFlow while resolving
185 subtle sub-populations (T et al., 2021). We used the clustering algorithm FlowSOM (Van Gassen et al.,
186 2015) followed by optimized t-stochastic neighbor embedding (opt-SNE) (Belkina et al., 2019) (Details
187 about the parameters used in FlowSOM and opt-SNE can be found in Supplementary File 3). We first

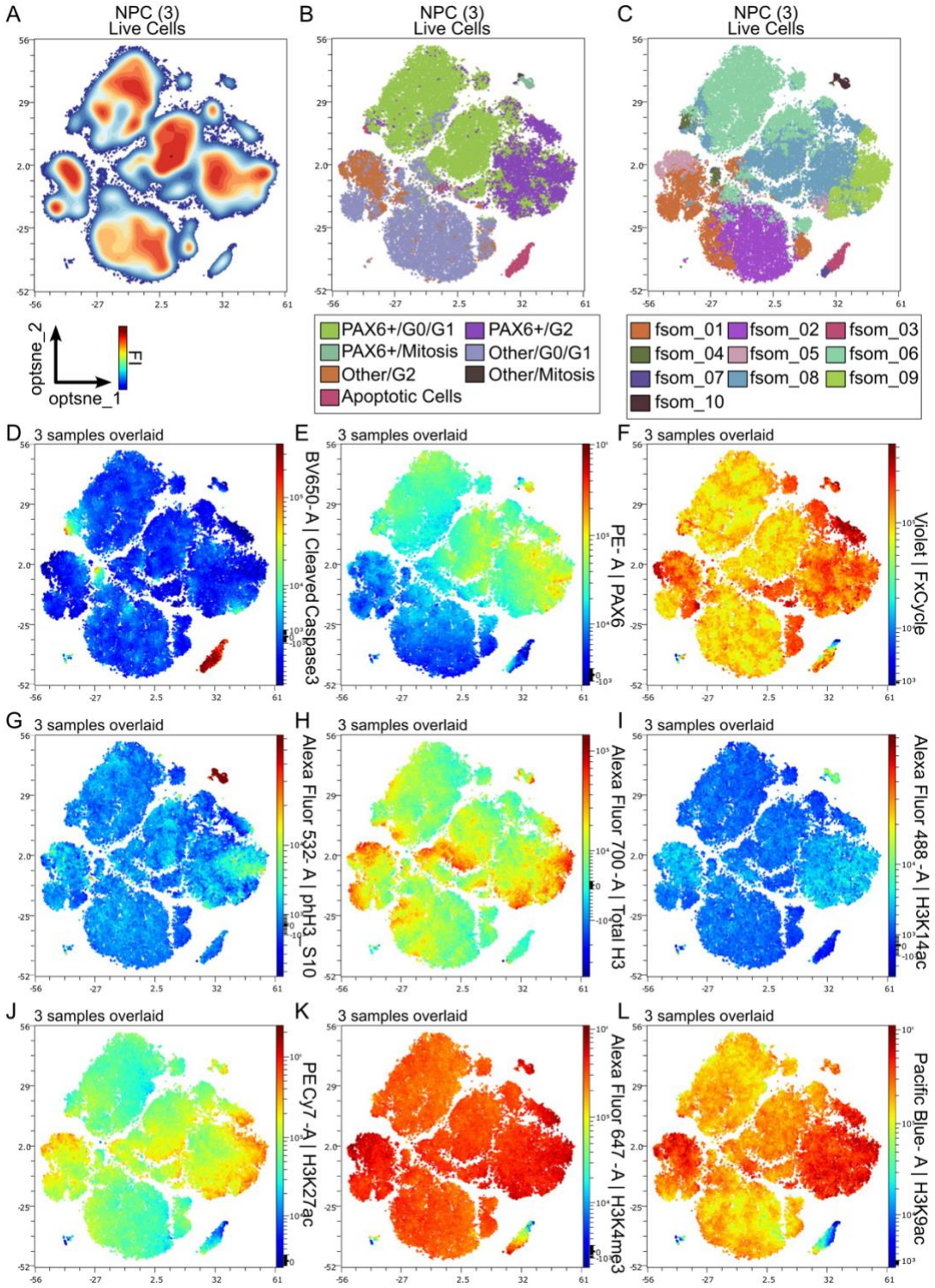

Figure 2. Visualization of manual gating and unsupervised clustering in the opt-SNE two-dimensional space. (A) opt-SNE density plot of concatenated spectral flow data and reference (n = 3). (B) Traditional two-dimensional gating is visualized in the opt-SNE dimensions (C) Curated FlowSOM clusters are visualized in the opt-SNE two-dimensional space. (D-L) Fluorescence intensity values of each feature were plotted as a color-continuous color in the two opt-SNE dimensions. The fluorescence intensity (FI) scale for each feature shows blue for low intensity, green/yellow for medium intensity and red for high intensity.

evaluated the quality of the FlowSOM clusters by comparing them with traditional gates in the opt-SNE two-

189 dimensional space (Fig. 2 A-C). To assess if the obtained clusters were consistent with expected histone
190 patterns (Li et al., 2005; Yiyuan Liu et al., 2017; Ma et al., 2015; Park et al., 2022; Pelham-Webb et al.,
191 2021; Sze et al., 2017; Van Rechem et al., 2021), we inspected the distribution and intensity of each feature
192 by plotting them in a color-continuous scale in the opt-SNE graphs (Fig. 2, D-L). Our analysis resulted in 11
193 FlowSOM elbow metaclusters that, after careful exploration of all features, were consolidated into 10
194 clusters (Fig. 2, C; fsom clusters 01-10. For details on merged clusters, see Supplementary File 3).
195 Unsupervised clustering resolved the expected cell populations (Fig.2 D-G) and identified unique cell states
196 or clusters that could potentially be driven by distinct histone H3 PTM patterns (Fig. 2 C, H-L). Notably, it
197 also generated an artificial cluster, potentially arising from technical or computational artifacts, highlighting
198 the need for manual inspection of clusters and transparent reporting of the analysis.

199 Visualization of clusters and features in a two-dimensional space can be useful for initial feature
200 exploration of spectral flow cytometry data. However, the axis and global distances in these plots are
201 meaningless and are not exempt from data distortion shortcomings reported in transcriptional data analysis
202 (Chari and Pachter, 2023; T et al., 2021). To validate the sensitivity and resolution power of EpiFlow we
203 further investigated whether each cluster represented a true cell population and assessed the possible
204 contributions of histone H3 PTMs to a given cell state. We evaluated the relative contribution of all features
205 to each cluster, the distribution of fluorescence intensity values of all H3 PTMs within a cluster, and the
206 correlation between features and clusters. In this article, we use as example clusters fsom_08 and fsom_09
207 that showed similar levels of expression of PAX6 (known NPC) and DNA content (FxCycle denoting cells
208 in G2) with subtle differences in fluorescence intensity values for H3 PTMs. Cluster 10 is also exemplified
209 due to its unique signature in all features (PAX6 positive, phH3_S10 positive representing mitotic NPC)
210 (Fig. 3. For a complete analysis of all clusters, refer to the associated GitHub Repository). Our analysis
211 showed that NPCs in clusters 08 and 09 had the same five leading features (FxCycle, PAX6, H3K4me3,
212 H3K9ac, and H3K27ac), but PAX6 and H3K27ac contributed differently to each cluster (Fig. 3 A, B. Each
213 bar is ordered counterclockwise from higher to lower contribution). Additionally, while H3K9ac had the same
214 relative contribution to both clusters (Fig. 3 A, B; third bar), it had a unique distribution of fluorescence
215 intensity values in each cluster (Fig. 3 C, E). Our statistical analysis showed a significant difference in the
216 fluorescence intensity and distribution of H3K4me3, H3K9ac, H3K14ac, and H3K27ac across clusters,
217 suggesting their potential role in distinguishing the biological state of the cells within each cluster (Fig. 3,
218 G-J, Dunn pairwise test for selected clusters. Fig. S5, Krustal-Wallis test for all clusters. For a complete
219 analysis of all clusters, refer to the associated GitHub Repository). When H3 PTM and cell cycle features
220 are assessed within each cluster, we observed significant differences across all clusters, suggesting that
221 they represent a distinct cellular state of NPCs with varying fluorescence intensity distributions of the
222 analyzed features (Fig. S6).

223 Our work demonstrates that EpiFlow can be used to resolve subtle patterns of histone H3 PTM across
224 cell cycle phases with high resolution. With careful panel design, EpiFlow has the potential to explore the
225 relationship between histone PTMs, transcription factors, and lineage commitment in varying cell types and

samples (cell cultures, organoids, biopsies). Moreover, through the associated GitHub repository, we provide a reproducible and accessible workflow for the exploratory and statistical analysis presented in this article. With this work, we hope to facilitate the application of EpiFlow and its data analysis.

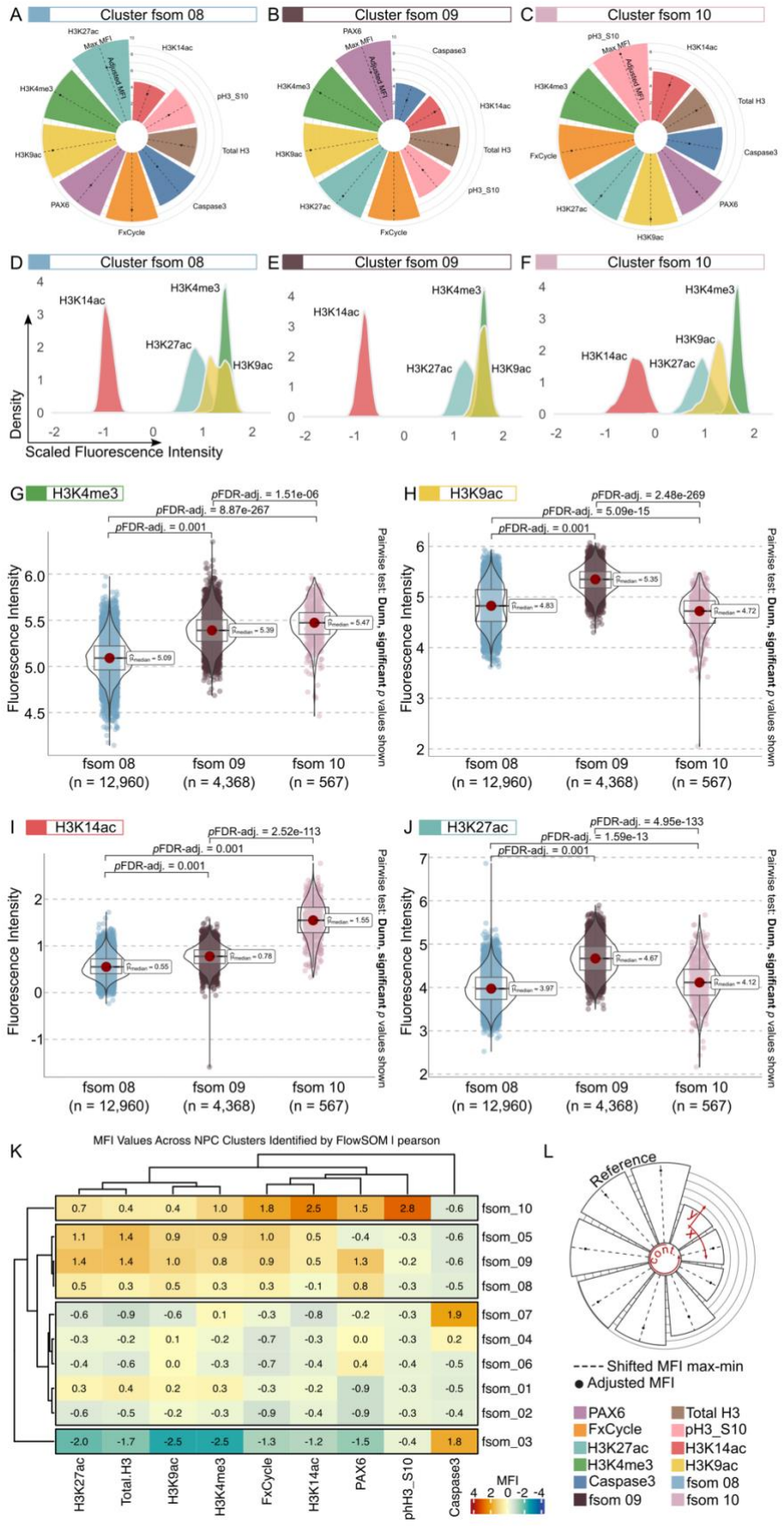
A
Cluster fsom 08
B
Cluster fsom 09
C
Cluster fsom 10
H3K27ac
Max MFI
Adjusted MFI
H3K14ac
pH3_S10
Total H3
Caspase3
FxCycle
PAX6
H3K9ac
H3K4me3
H3K8ac
D
Cluster fsom 08
E
Cluster fsom 09
F
Cluster fsom 10
Density
Scaled Fluorescence Intensity
G
H3K4me3
pFDR-adj. = 1.51e-06
pFDR-adj. = 8.87e-267
pFDR-adj. = 0.001
H
H3K9ac
pFDR-adj. = 2.48e-269
pFDR-adj. = 5.09e-15
pFDR-adj. = 0.001
I
H3K14ac
pFDR-adj. = 2.52e-113
pFDR-adj. = 0.001
pFDR-adj. = 0.001
J
H3K27ac
pFDR-adj. = 4.95e-133
pFDR-adj. = 1.59e-13
pFDR-adj. = 0.001
Fluorescence Intensity
Pairwise test: Dunn, significant p values shown
fsom 08
(n = 12,960)
fsom 09
(n = 4,368)
fsom 10
(n = 567)
K
MFI Values Across NPC Clusters Identified by FlowSOM | pearson
fsom_10
fsom_05
fsom_09
fsom_08
fsom_07
fsom_04
fsom_06
fsom_01
fsom_02
fsom_03
H3K27ac
Total.H3
H3K9ac
H3K4me3
FxCycle
H3K14ac
PAX6
phH3_S10
Caspase3
MFI
L
Reference
Cont.
Shifted MFI max-min
Adjusted MFI
PAX6
FxCycle
H3K27ac
H3K4me3
Caspase3
fsom 09
Total H3
pH3_S10
H3K14ac
H3K9ac
fsom 08
fsom 10

Figure 3. High-dimensional data exploration and assessment of H3-PTM profiles across clusters in NPCs. Data analysis and visualization strategies to evaluate feature contributions and distributions to each cluster and assess H3-PTM signatures. (A-C) Circular bar plots highlighting the contribution of each feature in selected clusters. Median Fluorescence Intensity (MFI) values were transformed so that all values are positive and greater than zero [MFI shifted = mfi + abs(min(mfi)) + 1]. Values are then summarized by feature (colored bars) within each cluster displaying maximum (outer end of the bar), minimum (inner end of the bar), and median values (shifted MFI, dot in the midline of each bar). Features (bars) are ordered from larger to smaller MFI values in a counterclockwise direction to highlight their contributions to each cluster. (D-F) Density plots showing H3-PTMs scaled fluorescence intensity values and distributions in each cluster. (G-J) Violin plots of fluorescence intensity for H3K4me3 (G), H3K9ac (H), H3K14ac (I), and H3K27ac (J) across fsom_08, fsom_09, and fsom_10. Dunn pairwise test, statistically significant *p*-values shown. (K) Heatmap showing the MFI values across 10 NPC clusters identified. To assess the correlation between H3-PTM, cell cycle status, and expression levels of PAX6, clustering of scaled MFI values (displayed within the heatmap) was performed using the Pearson correlation distance method. (L) Reference cartoon to support the interpretation of circular bar plots and color-code of each feature.

Limitations of this study

While EpiFlow can resolve very subtle differences in fairly homogenous cell populations, assigning labels or identities to clusters is limited by the markers used in the panel, such as PAX6 or DNA content for cell cycle phases. Furthermore, EpiFlow does not provide genomic information on the histone marks nor link these modifications to specific chromatin regions or regulatory elements. Therefore, inferring the biological relevance of a given cluster with a distinct histone H3-PTM profile is not possible without downstream approaches and validation.

Technical notes

Panel design and optimization are two of the most critical steps in spectral flow cytometry experiments, as they ensure sensitivity and reproducibility of results. Below, we provide general guidelines to support Epiflow implementation with different cell types and markers. However, we strongly advise the reader to consult the available literature for optimal spectral flow cytometry experimental design and downstream analysis (den Braanker et al., 2021; Ferrer-Font et al., 2021; Fox et al., 2020; Park et al., 2020; T et al., 2021).

1. The guidelines for assigning fluorochromes to the antigen of interest used for traditional flow cytometry still apply to spectral flow cytometry. Match brighter fluorochromes with lowly expressed antigens. Co-expressed antigens should be assigned colors that have distinct spectra with low spread. If possible, consider using fluorochromes with high spillover spread or emitting in the autofluorescent channels (~500 nm) for positive events that get removed, like the viability stain.

2. Panel design can be supported using www.FluoroFinder.com. Ideally, build a panel with a low complexity index. This readout indicates how noisy the data will be given how similar the fluorochrome spectra are to each other.

3. Although not discussed in this protocol, it is critical to titrate each antibody on the target cell type before running the final panel to ensure that the signal is within range. This is also true for new antibody lots and

257 clones. The histone antibodies were not originally titrated for this protocol as the signal was in range of the
258 detectors (add drug experiments).

259 4. Utilizing isotype controls is a debated topic in this field (Andersen et al., 2016; Keeney et al., 1998). We
260 did not use isotype controls in this work because we previously titrated our antibodies and confirmed that
261 the assay was sensitive and specific (Fig. S2, S3, S8).

262 5. Autofluorescent spectral signatures will be unique to each cell type and can change depending on
263 factors related to cell stress and metabolism.

264 6. To ensure statistical power, capture at least 5,000 bead events and 10,000 cell events.

265 7. Unmixing controls vary depending on the sample. It's important to compare unmixing results using
266 beads and cells before selecting the most appropriate option. For further details, please refer to Ferrer-Font
267 et al. 2021[11].

268 8. Several factors can contribute to variability in spectral flow assays.

269 a. Sample preparation: Inconsistent cell counts, temperature control, inadequate mixing, and improper
270 storage conditions.

271 b. Bead preparation: To generate spectra that are comparable, beads and cells must be treated
272 identically. Any differences in processing or staining sequences can lead to beads binding antibodies
273 differently than cells, producing spectral signatures that may not accurately represent the cell
274 populations.

275 c. Aurora daily quality control (QC): Calibration of the Aurora is essential after startup to ensure optimal
276 performance. Before acquiring data, confirm that the Daily QC check has passed. This ensures that
277 optical alignment, laser delays, scaling factors, gain settings, and performance drift are optimized to
278 account for daily instrument variability.

279 9. Excessive dead cells and debris can arise from rough handling before viability staining, missed wash
280 steps, or from introducing bubbles during pipetting in 96-well plates. To minimize cell shearing, handle live
281 cells gently and avoid pipetting volumes exceeding 100 µL in 96-well plates to prevent introducing air.
282 Additionally, perform all wash steps as outlined in the protocol to ensure thorough washing (Protocols S1
283 and S2).

284 10. Cross-contamination of spectral signatures between neighboring wells can happen due to slow plate
285 decanting. To avoid this, decant quickly and swiftly (≤1 second) to ensure pellets remain at the well base
286 and prevent droplets from migrating to adjacent wells.

287 11. Excessive doublet populations can result from inadequate mixing during pellet resuspension or
288 prolonged storage at 4 °C. To address this, consider passing cells through a 0.45 µm filter and improving
289 sample mixing by setting the pipette to a larger volume setting of ~70-80 µL. Also, try mixing samples
290 immediately before analysis and avoid overnight storage of methanol-treated cells to prevent stickiness.

291

292 **Materials and methods**

293 The SCTi003-A (RRID:CVCL_C1W7) and WTC11 (UCSFi001-A, RRID:CVCL_Y803) control hiPSC
294 lines were used throughout this study. Room temperature refers to 22 °C. All hiPSC lines were karyotyped
295 and confirmed to be free of mycoplasma. The complete step-by-step protocol, including reagent
296 concentrations and recipes can be found in Protocol S1. Importantly, this protocol can be applied to samples
297 run on traditional flow cytometers, including the Stratedigm S1000EXi benchtop flow cytometer. For this,
298 the panel design process should be repeated to ensure that the fluorochromes selected are compatible
299 with the instrument. Details on the Stratedigm assays are in Protocol S2, Table S2. All experiments were
300 conducted as n=3 biological triplicates. ChatGPT4o (AI) was used to assist in text refinement and code
301 optimization.

302 **Cell culture**

303 hiPSCs were grown on 6-well plates (Corning) coated with 2D Matrigel (Corning) in mTeSR Plus media
304 (Stem Cell Technologies) supplemented with Primocin (InvivoGen). Once the cells were ~70% confluent,
305 the media was replaced with STEMdiff SMADi Neural Induction media (Stem Cell Technologies)
306 supplemented with Primocin. The neural induction was performed following the manufacturer's protocol.
307 Cells were subcultured at 70% confluency to maintain continuous mitosis events by day 7. All cultures were
308 incubated at 37°C in a 5% CO2 incubator with daily media changes.

309 **Drug Treatments**

310 NPCs were cultured to 70% confluency and treated with three different concentrations of Trichostatin
311 A (TSA; 0.5μM, 1μM, 10μM) or A485 (1μM, 10μM, 20μM). SCTi-003A hiPSCs were also grown to 70%
312 confluency and treated with TSA (0.5μM, 1μM, 2μM) or Vorinostat (SAHA; 0.5μM, 0.75μM,1μM). Cells were
313 treated for 4 hours with either the drug or DMSO, then harvested and processed according to the flow
314 cytometry protocols outlined above.

315 **Sample preparation**

316 On day 7 NPCs were gently detached and resuspended in a round bottom 96-well plate. Cell pellets
317 were stained with fixable viability dye (BD) for 15 minutes on a rotating platform at room temperature. Cells
318 were then fixed in 4% PFA (Thermo Fisher) for 20 minutes at room temperature. For permeabilization, cells
319 were incubated with 100% ice-cold methanol (Fisher Chemical) for 15 minutes in a -20°C freezer. For
320 blocking, cells were incubated with 5% BSA for 30 minutes on a rotating platform at room temperature.
321 Cells were then incubated with the appropriate antibody cocktail for 1 hour on a rotating platform at room
322 temperature. Finally, cells were stained with FxCycle Flow Ready (Invitrogen) for 30 minutes on a rotating
323 platform at room temperature. FxCycle was not removed from the solution prior to running on the cytometer.
324 All incubations were performed with a shaking speed of ~80 rpm. Between each step (except FxCycle),
325 cells were washed once in FACs buffer (0.5% BSA (Sigma-Aldrich)). All centrifugal spins were performed
326 at 4°C for 5 minutes. Following the spin, a quick and swift decanting movement was used to ensure that
327 sample loss and cross-contamination were prevented. Single color controls (SCCs) were prepared using

328 beads (Invitrogen) or cells. Cells were used for all dye-based staining. After dyes and antibodies were
329 added, the samples were protected from light using foil.

330 **Spectral flow cytometry assay**

331 Data was acquired on a 5L Cytek Aurora analyzer (Cytek Biosciences). Before acquiring the data,
332 ensure that each sample is well-mixed by pipetting immediately before running the assay. Ensure that the
333 Aurora completed the warmup/start-up initialization and passed the quality control check. Run the spectral
334 flow cytometry assay according to user-defined settings. We utilized the following acquisition settings for
335 NPCs: Events to record: 10,000,000, Stopping time (sec): 10,000, Stopping volume (μL): 150, Flow rate:
336 High, FSC: 40, SSC: 20.

337 **Data unmixing**

338 Acquired data was unmixed with SpectroFlo v2 (Cytek Biosciences) without autofluorescence removal.
339 Unstained cells and SCCs (beads or cells) were used as references for unmixing, as detailed in Table S1.
340 After unmixing, both SCCs and fully stained samples were manually inspected for potential unmixing
341 artifacts in NxN plots (File S2) following recommended guidelines for spectral flow cytometry panel
342 optimization (Ferrer-Font et al., 2021).

343 **Gating, clustering and dimensionality reduction**

344 The data analysis workflow for gating and dimensionality reduction was built using the cloud-based OMIQ
345 analysis platform (File S3). To ensure all events were properly scaled, each feature was transformed using
346 arcsinh (File S3). Three gating strategies were implemented to optimize signal separation, exclude artifacts
347 or debris, and identify distinct cell populations, ensuring accurate downstream analysis.

348 *Event rate and cell quality gating:* First, time gating was applied to select events recorded with a stable
349 flow rate. This was followed by additional gating to isolate singlets, exclude debris, and discriminate live
350 and dead cells. Subsequent gating and analyses were performed within the live cell population.

351 *Manual gating as a benchmark:* This strategy involved the identification of apoptotic cells (cleaved
352 Caspase-3 positive cells), neuronal progenitor cells (PAX6 positive cells), and determining cell cycle status
353 (G0/G1-G2: FxCycle; mitosis: pH3-S10 positive cells). To account for differences in fluorescence intensity
354 signal observed in H3K9ac, H3K4me3, H3K14ac, and H3K27ac features, distinct gates were applied
355 targeting events with low, medium, and high fluorescence intensity within each cell cycle phase. Changes
356 in global H3 were assessed across G0/G1, G2, and mitosis. Fluctuations in H3-PTM fluorescence intensity,
357 potentially driven by H3 replication-dependent biogenesis (Armstrong and Spencer, 2021), were evaluated
358 by applying specific gates for each histone mark within the Total H3 gate (Fig. S7). After manual gating, the
359 subset of fully stained files was retained and the maximum number of live cells was randomly subsampled
360 from each replicate.

361 *Unsupervised clustering and gating:* Unsupervised clustering was performed using FlowSOM (Van
362 Gassen et al., 2015). The resulting elbow meta-clusters ("fsom clusters"), representing distinct groupings
363 of data that share similar characteristics, were embedded as gates for further analysis and comparison with

manual gating. Dimensionality reduction was performed using optimized T-distributed stochastic neighbor embedding (opt-SNE) (Belkina et al., 2019). Data was exported from OMIQ and is available in the GitHub repository associated with this article. Please refer to File S3 for a detailed workflow, including feature selection, analysis parameters, and random seed details for each algorithm.

Data exploration and visualization

The data exploration and visualization workflow was built in R using the renv package (Renv v1.0.7), which creates reproducible R environments and ensures data analysis reproducibility. This workflow provides a graphical representation of the main features contributing to each FlowSOM cluster. Methods and statistical analyses are described in the figure legends. A comprehensive analysis and data visualization code, including input data, data processing steps, and visualization rationale, is available at [https://github.com/SerranoLab/Golden_etal_2024].

Acknowledgments

The authors would like to thank Dr. Shari Brezinsky for instrumental support, Irena Feng for supporting initial method optimization, and Sandeep Sreerama and Sandra Sulser for sample processing support. We thank Dr. Effie Apostolou for helpful discussions and revisions of the project.

This work was supported by the Center for Regenerative Medicine and Boston University Chobanian & Avedisian School of Medicine through start-up funds to M.A.S. This work was also supported by the Flow Cytometry Core Facility at Boston University. hiPSC lines WTC11 and KMT2D10.4 were provided by grant UM1 HL098160 to HJY from the National Heart, Lung, and Blood Institute.

Competing Interests

The authors declare no competing interests.

Data and resource availability

Data analysis code and details of R packages used are available in [https://github.com/SerranoLab/Golden_etal_2024]. Raw flow cytometry and unmixed spectral flow cytometry data will be made available in FlowRepository.

References

Andersen, M.N., Al-Karradi, S.N.H., Kragstrup, T.W., Hokland, M., 2016. Elimination of erroneous results in flow cytometry caused by antibody binding to Fc receptors on human monocytes and macrophages. Cytometry Pt A 89, 1001–1009. https://doi.org/10.1002/cyto.a.22995

Armenta-Castro, E., Reyes-Vallejo, T., Máximo-Sánchez, D., Herrera-Camacho, I., López-López, G., Reyes-Carmona, S., Conde-Rodríguez, I., Ramírez-Díaz, I., Aguilar-Lemarroy, A., Jave-Suárez, L.F., Milflores-Flores, L., Santos-Lopez, G., Reyes-Leyva, J., Vallejo-Ruiz, V., 2020. Histone H3K9

and H3K14 acetylation at the promoter of the LGALS9 gene is associated with mRNA levels in cervical cancer cells. FEBS Open Bio 10, 2305–2315. https://doi.org/10.1002/2211-5463.12973

Armstrong, C., Spencer, S.L., 2021. Replication-dependent histone biosynthesis is coupled to cell-cycle commitment. Proceedings of the National Academy of Sciences 118, e2100178118. https://doi.org/10.1073/pnas.2100178118

Belkina, A.C., Ciccolella, C.O., Anno, R., Halpert, R., Spidlen, J., Snyder-Cappione, J.E., 2019. Automated optimized parameters for T-distributed stochastic neighbor embedding improve visualization and analysis of large datasets. Nat Commun 10, 5415. https://doi.org/10.1038/s41467-019-13055-y

Bergamasco, M.I., Vanyai, H.K., Garnham, A.L., Geoghegan, N.D., Vogel, A.P., Eccles, S., Rogers, K.L., Smyth, G.K., Blewitt, M.E., Hannan, A.J., Thomas, T., Voss, A.K., 2024. Increasing histone acetylation improves sociability and restores learning and memory in *KAT6B*-haploinsufficient mice. J Clin Invest 134. https://doi.org/10.1172/JCI167672

Bui, H.-T., Wakayama, S., Kishigami, S., Park, K.-K., Kim, J.-H., Thuan, N.V., Wakayama, T., 2010. Effect of Trichostatin A on Chromatin Remodeling, Histone Modifications, DNA Replication, and Transcriptional Activity in Cloned Mouse Embryos1. Biology of Reproduction 83, 454–463. https://doi.org/10.1095/biolreprod.109.083337

Calder, A., Roth-Albin, I., Bhatia, S., Pilquil, C., Lee, J.H., Bhatia, M., Levadoux-Martin, M., McNicol, J., Russell, J., Collins, T., Draper, J.S., 2013. Lengthened G1 Phase Indicates Differentiation Status in Human Embryonic Stem Cells. Stem Cells and Development 22, 279–295. https://doi.org/10.1089/scd.2012.0168

Chari, T., Pachter, L., 2023. The specious art of single-cell genomics. PLOS Computational Biology 19, e1011288. https://doi.org/10.1371/journal.pcbi.1011288

Coronado, D., Godet, M., Bourillot, P.-Y., Tapponnier, Y., Bernat, A., Petit, M., Afanassieff, M., Markossian, S., Malashicheva, A., Iacone, R., Anastassiadis, K., Savatier, P., 2013. A short G1 phase is an intrinsic determinant of naïve embryonic stem cell pluripotency. Stem Cell Research 10, 118–131. https://doi.org/10.1016/j.scr.2012.10.004

Crump, N.T., Hazzalin, C.A., Bowers, E.M., Alani, R.M., Cole, P.A., Mahadevan, L.C., 2011. Dynamic acetylation of all lysine-4 trimethylated histone H3 is evolutionarily conserved and mediated by p300/CBP. Proceedings of the National Academy of Sciences 108, 7814–7819. https://doi.org/10.1073/pnas.1100099108

den Braanker, H., Bongenaar, M., Lubberts, E., 2021. How to Prepare Spectral Flow Cytometry Datasets for High Dimensional Data Analysis: A Practical Workflow. Front. Immunol. 12. https://doi.org/10.3389/fimmu.2021.768113

Ferrer-Font, L., Small, S.J., Lewer, B., Pilkington, K.R., Johnston, L.K., Park, L.M., Lannigan, J., Jaimes, M.C., Price, K.M., 2021. Panel Optimization for High-Dimensional Immunophenotyping Assays Using Full-Spectrum Flow Cytometry. Current Protocols 1, e222. https://doi.org/10.1002/cpz1.222

Fox, A., Dutt, T.S., Karger, B., Obregón-Henao, A., Anderson, G.B., Henao-Tamayo, M., 2020. Acquisition of High-Quality Spectral Flow Cytometry Data. Current Protocols in Cytometry 93, e74. https://doi.org/10.1002/cpcy.74

Golden, C., Williams, S., Serrano, M., 2024. Nuclear Histone 3 Post-Translational Modification Profiling in Whole Cells using Spectral Flow Cytometry [WWW Document]. URL https://github.com/SerranoLab/Golden_etal_2024 (accessed 9.30.24).

Grebien, F., Vedadi, M., Getlik, M., Giambruno, R., Grover, A., Avellino, R., Skucha, A., Vittori, S., Kuznetsova, E., Smil, D., Barsyte-Lovejoy, D., Li, F., Poda, G., Schapira, M., Wu, H., Dong, A., Senisterra, G., Stukalov, A., Huber, K.V.M., Schönegger, A., Marcellus, R., Bilban, M., Bock, C., Brown, P.J., Zuber, J., Bennett, K.L., Al-awar, R., Delwel, R., Nerlov, C., Arrowsmith, C.H., Superti-Furga, G., 2015. Pharmacological targeting of the Wdr5-MLL interaction in C/EBPα N-terminal leukemia. Nat Chem Biol 11, 571–578. https://doi.org/10.1038/nchembio.1859

Grigoryev, S.A., Bulynko, Y.A., Popova, E.Y., 2006. The end adjusts the means: Heterochromatin remodelling during terminal cell differentiation. Chromosome Res 14, 53–69. https://doi.org/10.1007/s10577-005-1021-6

Hansen, K.H., Bracken, A.P., Pasini, D., Dietrich, N., Gehani, S.S., Monrad, A., Rappsilber, J., Lerdrup, M., Helin, K., 2008. A model for transmission of the H3K27me3 epigenetic mark. Nat Cell Biol 10, 1291–1300. https://doi.org/10.1038/ncb1787

Herzenberg, Leonore A., Tung, J., Moore, W.A., Herzenberg, Leonard A., Parks, D.R., 2006. Interpreting flow cytometry data: a guide for the perplexed. Nat Immunol 7, 681–685. https://doi.org/10.1038/ni0706-681

Karmodiya, K., Krebs, A.R., Oulad-Abdelghani, M., Kimura, H., Tora, L., 2012. H3K9 and H3K14 acetylation co-occur at many gene regulatory elements, while H3K14ac marks a subset of inactive inducible promoters in mouse embryonic stem cells. BMC Genomics 13, 424. https://doi.org/10.1186/1471-2164-13-424

Keeney, M., Gratama, J.W., Chin-Yee, I.H., Sutherland, D.R., 1998. Isotype controls in the analysis of lymphocytes and CD34+ stem and progenitor cells by flow cytometry--time to let go! Cytometry 34, 280–283.

Krejčí, J., Uhlířová, R., Galiová, G., Kozubek, S., Šmigová, J., Bártová, E., 2009. Genome-wide reduction in H3K9 acetylation during human embryonic stem cell differentiation. Journal of Cellular Physiology 219, 677–687. https://doi.org/10.1002/jcp.21714

Kubo, N., Chen, P.B., Hu, R., Ye, Z., Sasaki, H., Ren, B., 2024. H3K4me1 facilitates promoter-enhancer interactions and gene activation during embryonic stem cell differentiation. Molecular Cell 84, 1742-1752.e5. https://doi.org/10.1016/j.molcel.2024.02.030

Kueh, A.J., Bergamasco, M.I., Quaglieri, A., Phipson, B., Li-Wai-Suen, C.S.N., Lönnstedt, I.M., Hu, Y., Feng, Z.-P., Woodruff, C., May, R.E., Wilcox, S., Garnham, A.L., Snyder, M.P., Smyth, G.K., Speed, T.P., Thomas, T., Voss, A.K., 2023. Stem cell plasticity, acetylation of H3K14, and *de novo* gene activation rely on KAT7. Cell Reports 42, 111980. https://doi.org/10.1016/j.celrep.2022.111980

Lab, S., 2024. Nuclear Histone 3 Post-translational Modification Profiling in Whole Cells using Spectral Flow Cytometry. Analysis Workflow.

Larson, J.L., Yuan, G.-C., 2012. Chromatin States Accurately Classify Cell Differentiation Stages. PLOS ONE 7, e31414. https://doi.org/10.1371/journal.pone.0031414

Lasko, L.M., Jakob, C.G., Edalji, R.P., Qiu, W., Montgomery, D., Digiammarino, E.L., Hansen, T.M., Risi, R.M., Frey, R., Manaves, V., Shaw, B., Algire, M., Hessler, P., Lam, L.T., Uziel, T., Faivre, E., Ferguson, D., Buchanan, F.G., Martin, R.L., Torrent, M., Chiang, G.G., Karukurichi, K., Langston, J.W., Weinert, B.T., Choudhary, C., de Vries, P., Kluge, A.F., Patane, M.A., Van Drie, J.H., Wang, C., McElligott, D., Kesicki, E., Marmorstein, R., Sun, C., Cole, P.A., Rosenberg, S.H., Michaelides, M.R., Lai, A., Bromberg, K.D., 2017. Discovery of a selective catalytic p300/CBP inhibitor that targets lineage-specific tumours. Nature 550, 128–132. https://doi.org/10.1038/nature24028

Lauberth, S.M., Nakayama, T., Wu, X., Ferris, A.L., Tang, Z., Hughes, S.H., Roeder, R.G., 2013. H3K4me3 Interactions with TAF3 Regulate Preinitiation Complex Assembly and Selective Gene Activation. Cell 152, 1021–1036. https://doi.org/10.1016/j.cell.2013.01.052

Lee, M.G., Wynder, C., Bochar, D.A., Hakimi, M.-A., Cooch, N., Shiekhattar, R., 2006. Functional Interplay between Histone Demethylase and Deacetylase Enzymes. Molecular and Cellular Biology 26, 6395–6402. https://doi.org/10.1128/MCB.00723-06

Li, D.W., Yang, Q., Chen, J.T., Zhou, H., Liu, R.M., Huang, X.T., 2005. Dynamic distribution of Ser-10 phosphorylated histone H3 in cytoplasm of MCF-7 and CHO cells during mitosis. Cell Res 15, 120–126. https://doi.org/10.1038/sj.cr.7290276

Liu, X., Guo, C., Leng, T., Fan, Z., Mai, J., Chen, J., Xu, J., Li, Q., Jiang, B., Sai, K., Yang, W., Gu, J., Wang, J., Sun, S., Chen, Z., Zhong, Y., Liang, X., Chen, C., Cai, J., Lin, Y., Liang, J., Hu, J., Yan, G., Zhu, W., Yin, W., 2023. Differential regulation of H3K9/H3K14 acetylation by small molecules drives neuron-fate-induction of glioma cell. Cell Death Dis 14, 1–14. https://doi.org/10.1038/s41419-023-05611-8

Liu, Yin, Chen, S., Wang, S., Soares, F., Fischer, M., Meng, F., Du, Z., Lin, C., Meyer, C., DeCaprio, J.A., Brown, M., Liu, X.S., He, H.H., 2017. Transcriptional landscape of the human cell cycle. Proceedings of the National Academy of Sciences 114, 3473–3478. https://doi.org/10.1073/pnas.1617636114

Liu, Yiyuan, Pelham-Webb, B., Di Giammartino, D.C., Li, J., Kim, D., Kita, K., Saiz, N., Garg, V., Doane, A., Giannakakou, P., Hadjantonakis, A.-K., Elemento, O., Apostolou, E., 2017. Widespread Mitotic Bookmarking by Histone Marks and Transcription Factors in Pluripotent Stem Cells. Cell Reports 19, 1283–1293. https://doi.org/10.1016/j.celrep.2017.04.067

Lo, W.-S., Trievel, R.C., Rojas, J.R., Duggan, L., Hsu, J.-Y., Allis, C.D., Marmorstein, R., Berger, S.L., 2000. Phosphorylation of Serine 10 in Histone H3 Is Functionally Linked In Vitro and In Vivo to Gcn5-

Mediated Acetylation at Lysine 14. Molecular Cell 5, 917–926. https://doi.org/10.1016/S1097-2765(00)80257-9

Ma, Y., Kanakousaki, K., Buttitta, L., 2015. How the cell cycle impacts chromatin architecture and influences cell fate. Front. Genet. 6. https://doi.org/10.3389/fgene.2015.00019

Novo, D., 2022. A comparison of spectral unmixing to conventional compensation for the calculation of fluorochrome abundances from flow cytometric data. Cytometry Pt A 101, 885–891. https://doi.org/10.1002/cyto.a.24669

Park, J., Lee, K., Kim, K., Yi, S.-J., 2022. The role of histone modifications: from neurodevelopment to neurodiseases. Sig Transduct Target Ther 7, 1–23. https://doi.org/10.1038/s41392-022-01078-9

Park, L.M., Lannigan, J., Jaimes, M.C., 2020. OMIP-069: Forty-Color Full Spectrum Flow Cytometry Panel for Deep Immunophenotyping of Major Cell Subsets in Human Peripheral Blood. Cytometry Part A 97, 1044–1051. https://doi.org/10.1002/cyto.a.24213

Pelham-Webb, B., Polyzos, A., Wojenski, L., Kloetgen, A., Li, J., Di Giammartino, D.C., Sakellaropoulos, T., Tsirigos, A., Core, L., Apostolou, E., 2021. H3K27ac bookmarking promotes rapid post-mitotic activation of the pluripotent stem cell program without impacting 3D chromatin reorganization. Molecular Cell 81, 1732-1748.e8. https://doi.org/10.1016/j.molcel.2021.02.032

Petruk, S., Sedkov, Y., Johnston, D.M., Hodgson, J.W., Black, K.L., Kovermann, S.K., Beck, S., Canaani, E., Brock, H.W., Mazo, A., 2012. TrxG and PcG Proteins but Not Methylated Histones Remain Associated with DNA through Replication. Cell 150, 922–933. https://doi.org/10.1016/j.cell.2012.06.046

Richon, V.M., Webb, Y., Merger, R., Sheppard, T., Jursic, B., Ngo, L., Civoli, F., Breslow, R., Rifkind, R.A., Marks, P.A., 1996. Second generation hybrid polar compounds are potent inducers of transformed cell differentiation. Proc Natl Acad Sci U S A 93, 5705–5708.

Roederer, M., Darzynkiewicz, Z., Parks, D.R., 2004. Guidelines for the presentation of flow cytometric data. Methods Cell Biol 75, 241–256. https://doi.org/10.1016/s0091-679x(04)75010-4

Ronzoni, S., Faretta, M., Ballarini, M., Pelicci, P., Minucci, S., 2005. New method to detect histone acetylation levels by flow cytometry. Cytometry Part A 66A, 52–61. https://doi.org/10.1002/cyto.a.20151

Seuter, S., Heikkinen, S., Carlberg, C., 2013. Chromatin acetylation at transcription start sites and vitamin D receptor binding regions relates to effects of 1α,25-dihydroxyvitamin D3 and histone deacetylase inhibitors on gene expression. Nucleic Acids Research 41, 110–124. https://doi.org/10.1093/nar/gks959

Sze, C.C., Cao, K., Collings, C.K., Marshall, S.A., Rendleman, E.J., Ozark, P.A., Chen, F.X., Morgan, M.A., Wang, L., Shilatifard, A., 2017. Histone H3K4 methylation-dependent and -independent functions of Set1A/COMPASS in embryonic stem cell self-renewal and differentiation. Genes Dev. 31, 1732–1737. https://doi.org/10.1101/gad.303768.117

T, L., Lm, W., Tm, A., N, S., M, P., S, V.G., F, M., 2021. An updated guide for the perplexed: cytometry in the high-dimensional era. Nature immunology 22. https://doi.org/10.1038/s41590-021-01006-z

Ushey, K., Wickham, H., 2024a. Introduction to renv [WWW Document]. URL https://rstudio.github.io/renv/articles/renv.html (accessed 9.30.24).

Ushey, K., Wickham, H., 2024b. rstudio/renv [WWW Document]. URL https://github.com/rstudio/renv, https://rstudio.github.io/renv/ (accessed 9.29.24).

Van Gassen, S., Callebaut, B., Van Helden, M.J., Lambrecht, B.N., Demeester, P., Dhaene, T., Saeys, Y., 2015. FlowSOM: Using self-organizing maps for visualization and interpretation of cytometry data. Cytometry Part A 87, 636–645. https://doi.org/10.1002/cyto.a.22625

Van Rechem, C., Ji, F., Chakraborty, D., Black, J.C., Sadreyev, R.I., Whetstine, J.R., 2021. Collective regulation of chromatin modifications predicts replication timing during cell cycle. Cell Reports 37, 109799. https://doi.org/10.1016/j.celrep.2021.109799

Vigushin, D.M., Ali, S., Pace, P.E., Mirsaidi, N., Ito, K., Adcock, I., Coombes, R.C., 2001. Trichostatin A Is a Histone Deacetylase Inhibitor with Potent Antitumor Activity against Breast Cancer in Vivo1. Clinical Cancer Research 7, 971–976.

Vinogradova, M., Gehling, V.S., Gustafson, A., Arora, S., Tindell, C.A., Wilson, C., Williamson, K.E., Guler, G.D., Gangurde, P., Manieri, W., Busby, J., Flynn, E.M., Lan, F., Kim, H., Odate, S., Cochran, A.G., Liu, Y., Wongchenko, M., Yang, Y., Cheung, T.K., Maile, T.M., Lau, T., Costa, M., Hegde, G.V., Jackson, E., Pitti, R., Arnott, D., Bailey, C., Bellon, S., Cummings, R.T., Albrecht, B.K., Harmange, J.-C., Kiefer, J.R., Trojer, P., Classon, M., 2016. An inhibitor of KDM5 demethylases reduces

survival of drug-tolerant cancer cells. Nat Chem Biol 12, 531–538. https://doi.org/10.1038/nchembio.2085

Weng, M.K., Zimmer, B., Pöltl, D., Broeg, M.P., Ivanova, V., Gaspar, J.A., Sachinidis, A., Wüllner, U., Waldmann, T., Leist, M., 2012. Extensive Transcriptional Regulation of Chromatin Modifiers during Human Neurodevelopment. PLOS ONE 7, e36708. https://doi.org/10.1371/journal.pone.0036708

Figure S1: Nuclear histone and membrane staining of SCTi-003A hiPSCs.

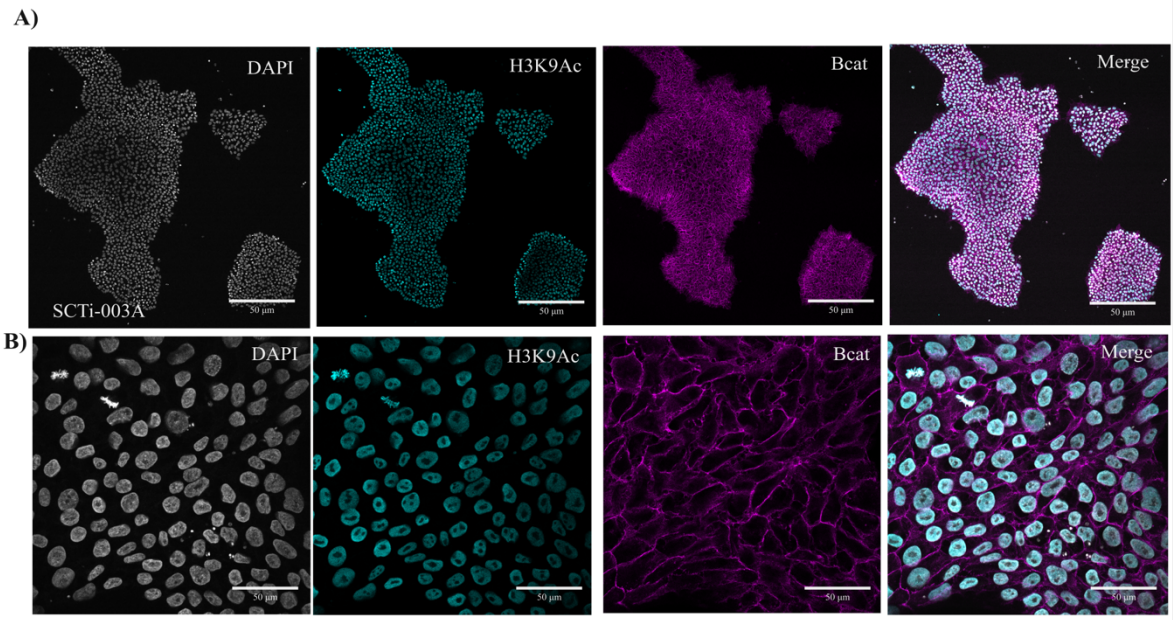

Figure S1: Immunofluorescent staining validation of cell membrane integrity and nuclear antigen identification. Confocal microscopy images of SCTi-003A hiPSCs. Colonies were fixed on glass coverslips and stained for β-catenin (Bcat) and histone 3 lysine 9 acetylation (H3K9ac) to assess membrane integrity and nuclear antigen location, respectively. (A) 10x magnification and (B) 63x magnification confocal images of SCTi-003A hiPSC colonies. Images were acquired on a Zeiss LSM 710 confocal microscope. Scale Bar: 50 μM.

Figure S2. Drug validation assay of spectral flow cytometry protocol

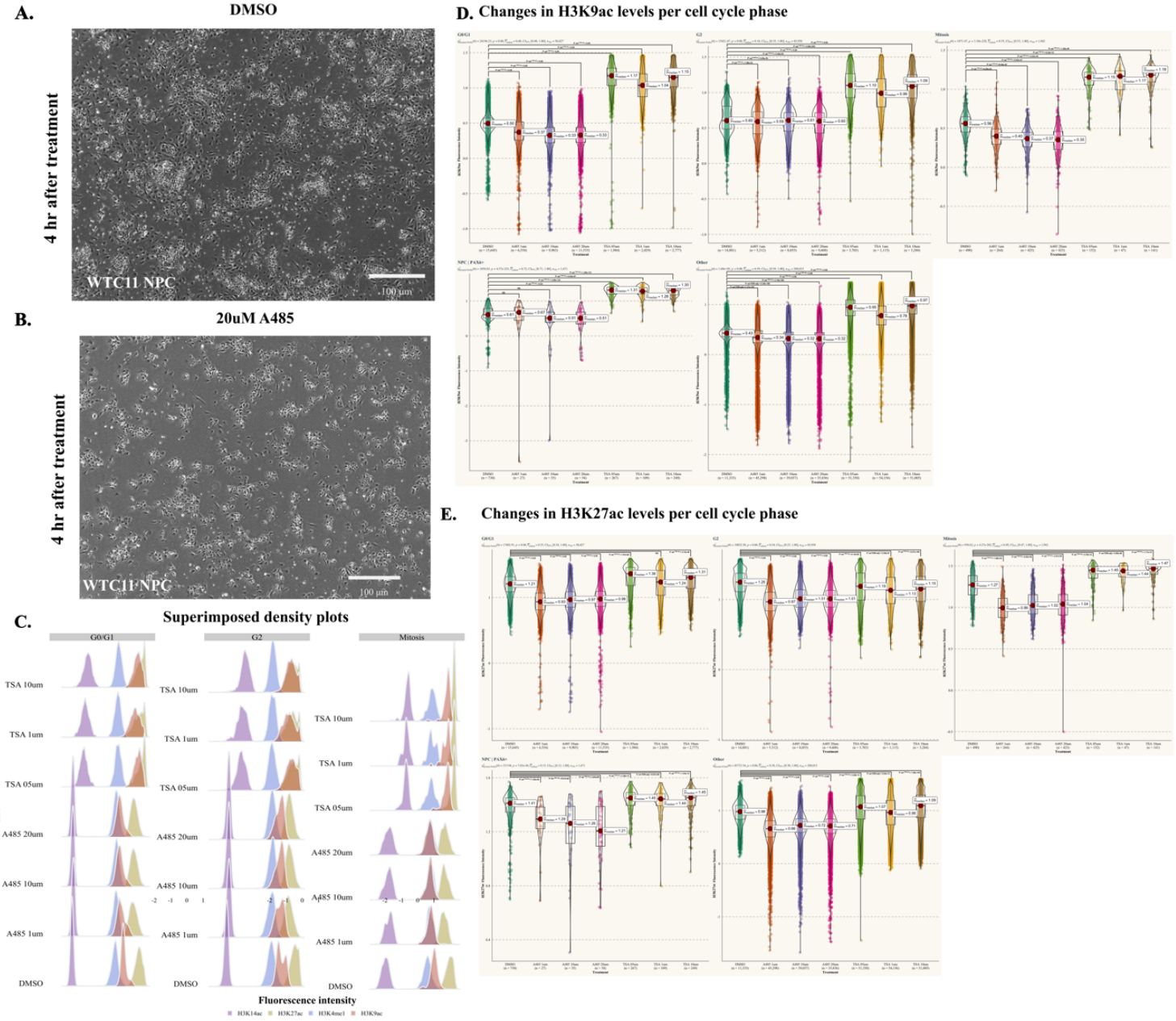

Figure S2. Validation of spectral flow cytometry protocol using epigenetic protein inhibitors. Spectral flow cytometry analysis of WTC11 NPC treated with TSA and A485. TSA is a histone deacetylase I/II inhibitor, resulting in increased histone acetylation. A485 is a histone acetyltransferase inhibitor that targets p300/CBP, resulting in reduced histone acetylation. For each drug treatment, cells were treated for 4 hours with DMSO (A), A485 (B), or TSA. A representative brightfield image from one concentration of A485 is shown. Superimposed density histogram plots across all drug concentrations for H3K9ac, H3K27ac, H3K4me1, and H3K14ac features show how the signal is distributed in each group across the cell cycle (C). Violin plots of the same groups confirm that the drugs were able to significantly alter H3-PTM acetylation levels (D, E). Replicates n=3 per group. Scale bar: 100 um. TSA: Trichostatin A. NPC: neural progenitor cells.

Figure S3. Drug validation assay of conventional flow cytometry protocol

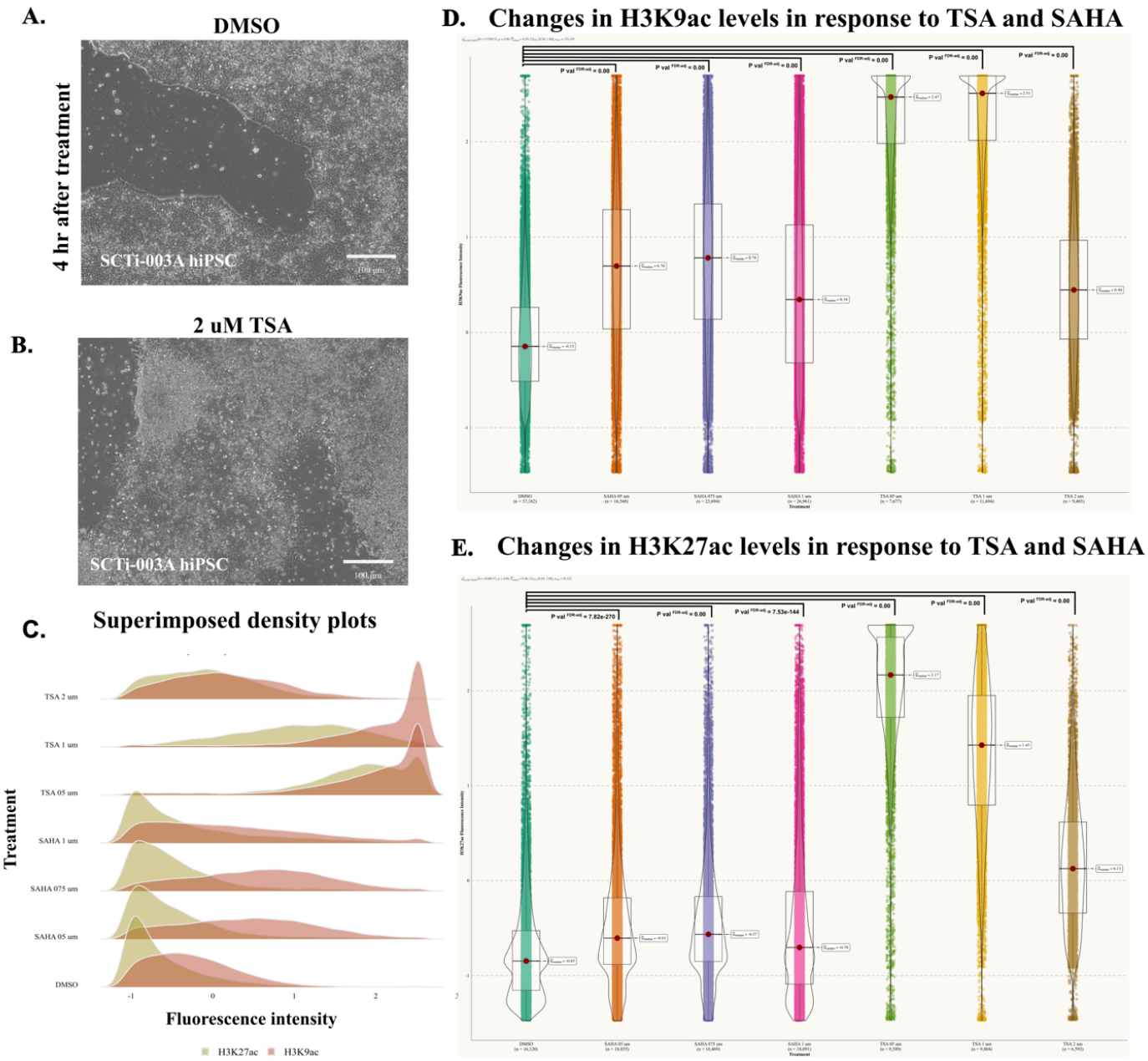

Figure S3. Validation of conventional flow cytometry protocol using epigenetic protein inhibitors. Conventional flow cytometry analysis of SCTi-003A hiPSCs treated with TSA and Vorinostat (SAHA). TSA and SAHA are histone deacetylase I/II inhibitors, resulting in increased histone acetylation. For each drug treatment, cells were treated for 4 hours with DMSO (A), TSA (B), or SAHA. A representative brightfield image from one concentration of SAHA is shown. Superimposed density histogram plots across all drug concentrations for H3K9ac and H3K27ac features show how the signal is distributed in each group (C). Violin plots of the same groups confirm that the drugs were able to significantly alter H3-PTM acetylation levels (D, E). Replicates n=3 per group. Scale bar: 100 um. TSA: Trichostatin A. SAHA: Vorinostat. hiPSC: human induced pluripotent stem cells.

Figure S4. Validation of EpiFlow to capture changes in histone H3 methylation levels.

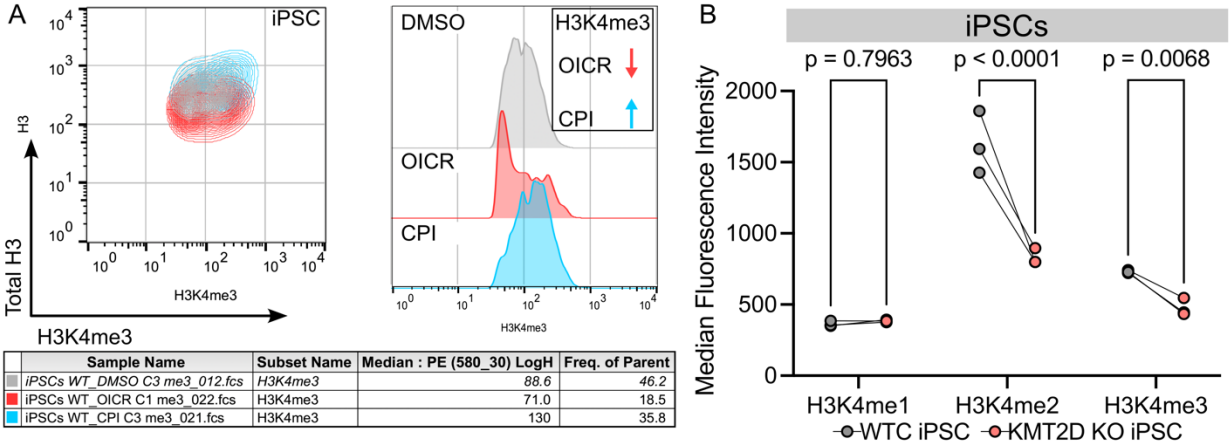

	Sample Name	Subset Name	Median : PE (580_30) LogH	Freq. of Parent
	iPSCs WT_DMSO C3 me3_012.fcs	*H3K4me3*	*88.6*	*46.2*
	iPSCs WT_OICR C1 me3_022.fcs	H3K4me3	71.0	18.5
	iPSCs WT_CPI C3 me3_021.fcs	H3K4me3	130	35.8

Figure S4. Results were obtained through multiparametric flow cytometry and analysis was performed in FlowJo. Median Fluorescence Intensity (MFI) values of each mark were calculated within the total H3 positive cells gate. **A.** To validate the specificity of EpiFlow to capture changes in H3K4me3 levels, wildtype iPSCs (WTC11) cells were treated with OICR and CPI to decrease or increase H3K4me3 marks, respectively. Table shows MFI values (median) of H3K4me3 in each experimental group: DMSO, 88.6; OICR, 71; CPI, 130. **B.** Validation of EpiFlow sensitivity using an iPSC line with a homozygous 2bp deletion loss of function (LOF) mutation in the histone methyl-transferase gene *KMT2D*. The *KMT2D* LOF iPSC cell line was generated with CRISPR/Cas9 technology targeting exon 2 of *KMT2D* in a WTC11 iPSC cell line. MFI (median) values of H3K4me1, H3K4me2 and H3K4me3 are plotted for three biological replicates per genotype. Ordinary 2way ANOVA: Interaction $p<0.0001$; Methylation mark $p<0.0001$; Genotype $p<0.0001$. Post hoc uncorrected Fisher's LSD p values from pairwise comparisons are shown.

Figure S5

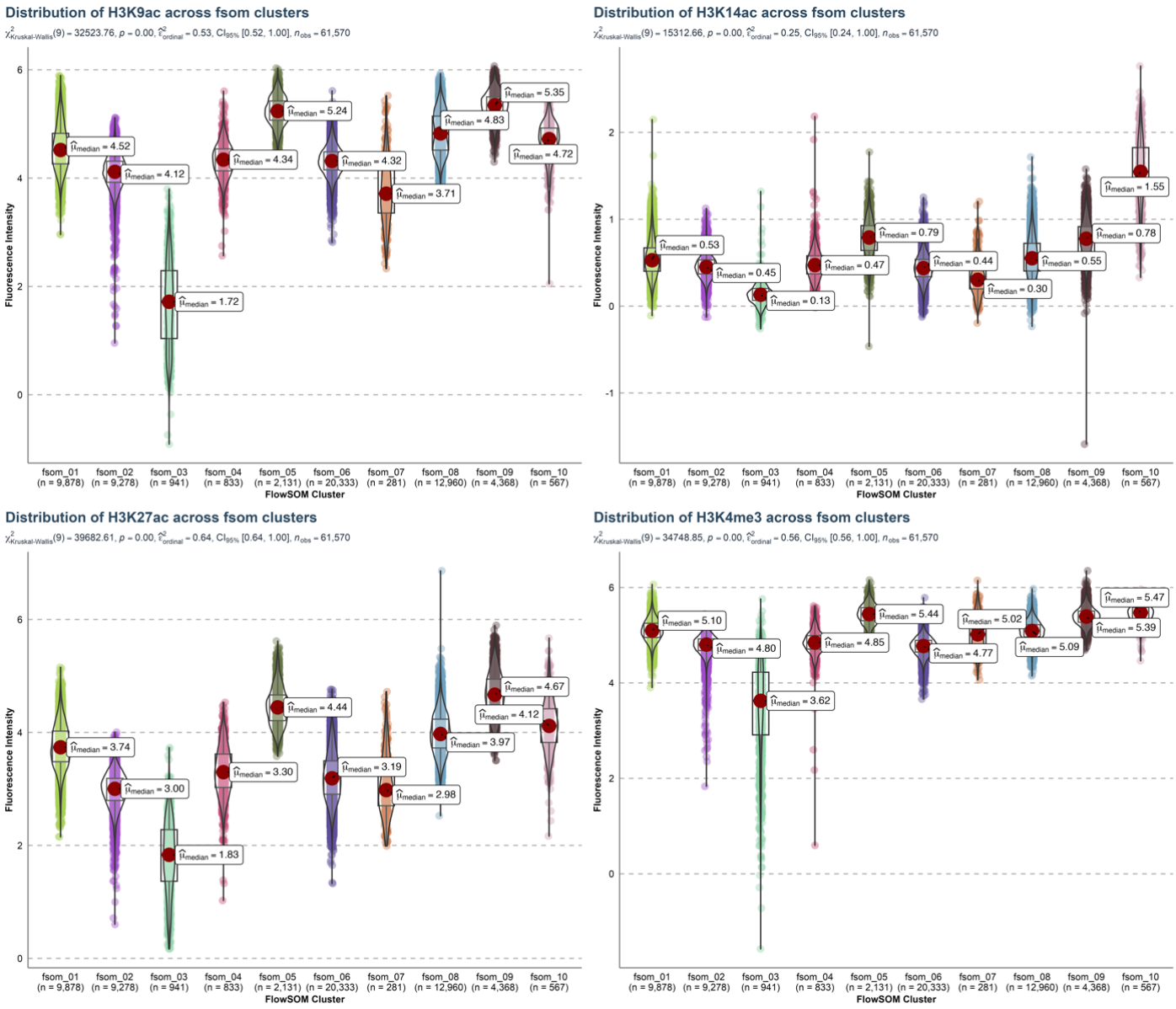

Figure S5. Distribution of H3 PTM fluorescence intensity in NPCs across 10 FlowSOM clusters. Violin plots of fluorescence intensity distributions for H3K9ac, H3K14ac, H3K27ac, and H3K4me3 across 10 clusters. Median values for each cluster are indicated with red dots, and their corresponding numerical values are labeled. Krustal-Wallis test shows significant differences in each feature assessed H3K9ac $\chi^2(9) = 32523.76$, $p<0.0001$; H3K14ac $\chi^2(9) = 15312.66$, $p<0.0001$; H3K27ac $\chi^2(9) = 39682.61$, $p<0.0001$; H3K4me3 $\chi^2(9) = 34748.85$, $p<0.0001$.

Figure S6

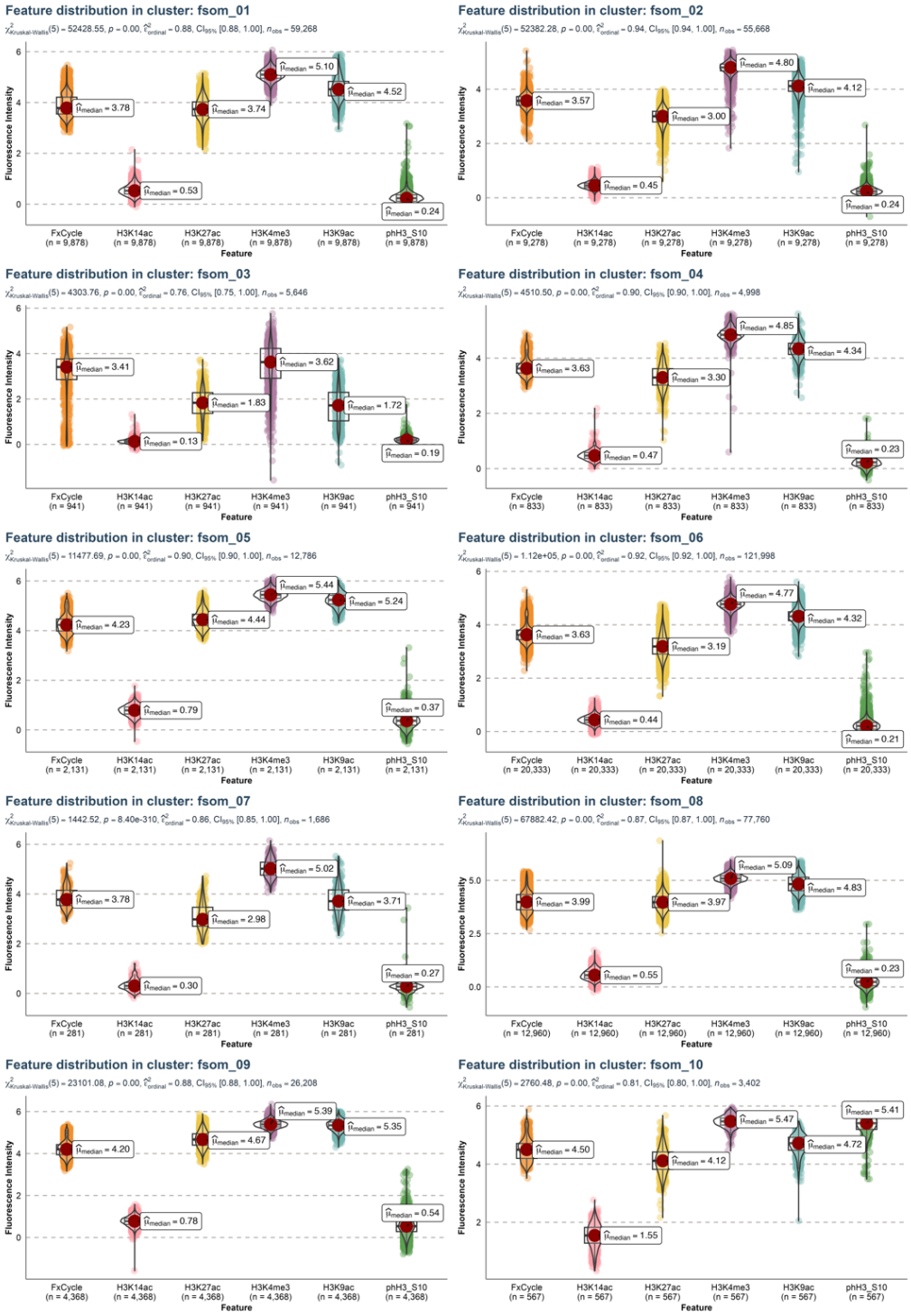

Figure S6. Assessment of H3 PTM signatures and cell cycle markers within clusters. Violin plots representing fluorescence intensity distributions of FxCycle, H3K14ac, H3K27ac, H3K4me3, H3K9ac, and phH3_S10 across 10 clusters (fsom_01 to fsom_10). Boxplots within each violin plot show the interquartile range and median fluorescence intensity values (red spot). Kruskal-Wallis test was applied to compare fluorescence intensities of all features within each cluster. Dunn's pairwise test was performed for post-hoc analysis. Sample sizes (n) are indicated for each feature in each cluster.

Supplementary Figure 7

Supplementary Figure 7: Comparison of Gating Strategies for H3 PTMs and Cell Cycle Markers Across G0/G1, G2, and Mitosis in NPCs. Violin plots of all features across gated cell populations in different cell cycle phases. Kruskal-Wallis test statistics and p-values are provided for each feature. Dunn pairwise comparisons are available in GitHub Repository.

Supplementary Figure S8

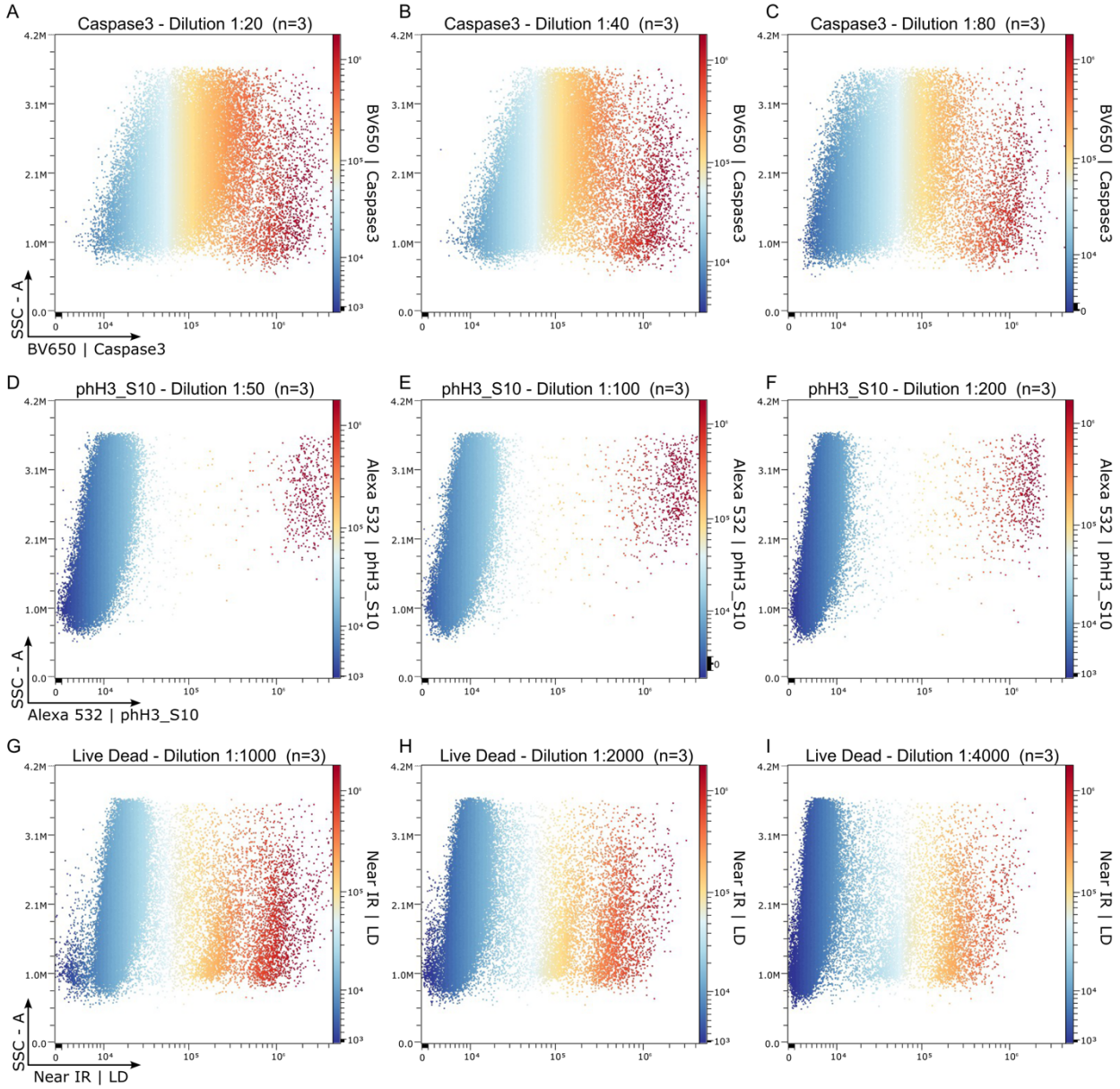

Supplementary Figure 8. Titration experiment for select reagents. A-C. Caspase3 antibody was titrated at 1:20, 1;40, and 1:80 dilutions. The 1:200 dilution was selected for experiments. D-F: Phospho-Histone H3 (Ser10) was titrated at 1:50, 1:100, and 1:200. A dilution of 1:400 was chosen for future experiments because the signal was still nearing the detection limits at the highest tested dilution. G-I. Live dead dye staining was titrated at 1:1,000, 1:2,000, and 1:4,000. Similar to phH3, a dilution of 1:8,000 for the Live/Dead stain was selected because the signal was still nearing the detection limits at the highest tested dilution.

Table S1. Spectral unmixing controls

Laser	Fluorochrome	Marker	Clone	Vendor	Catalog #	Unmixing
355	Violet	FxCycle/DNA	NA	Thermo Fisher	R37166	Cells
405	Pacific Blue	H3K9ac	C5B11	Cell Signaling	11857S	Beads
405	BV650	Active Caspase-3	C92-605.rMAb	BD	570179	Beads
405	mFluorViolet 500 SE	PAX6[(1)]	PAX6/1166	Novus Biologicals	47915MFV500	Beads
488	Alexa Fluor 488	H3K14ac	D4B9	Cell Signaling	26828	Beads
488	Alexa Fluor 532	PhosphoH3 (Ser10)	D2C8	Cell Signaling	52725	Beads
561	PE	PAX6[(2)]	O18-1330	BD	561552	Beads
561	PE	H3K4me1[(1)]	D1A9	Cell Signaling	55800S	Beads
561	PE-Cy7	H3K27ac	D5E4	Cell Signaling	30342	Beads
640	Alexa Fluor 647	H3K4me3[(2)]	C42D8	Cell Signaling	12064	Beads
640	Alexa Fluor 700	Total H3	D1H2	Cell Signaling	54826	Beads
640	Near IR 780	Fixable Viability	NA	BD	565388	Cells

[(1)] Included in the NPC panel for drug treatment validation assay **(Figure S3)**

[(2)] Excluded in the NPC panel for drug treatment validation assay **(Figure S3)**

Reagents

- Acetyl-Histone H3 (Lys9) (Cell Signaling Technologies, catalog number: 28036S)
- Acetyl-Histone H3 (Lys27) (Cell Signaling Technologies, catalog number: 15562S)
- Histone H3 647 (Cell Signaling Technologies, catalog number: 12230S)
- Mono-Methyl-Histone H3 (Lys4) (Cell Signaling Technologies, catalog number: 55800S)
- Di-Methyl-Histone H3 (Lys4) (Cell Signaling Technologies, catalog number: 31777S)
- Tri-Methyl-Histone H3 (Lys4) (Cell Signaling Technologies, catalog number: 62255S)

Table S1: Stratedigm Antibody Panel

Antibody	**Catalog Number**	**Dilution**	**Volume**	**FACs Buffer**	**Total volume**
Acetyl-Histone H3 (Lys9)*	28036S	1:50	12 μL	588 μL	600 μL
Histone H3 647*	12230S	1:50	12 μL	588 μL	600 μL
Acetyl-Histone H3 (Lys27)*	15562S	1:50	12 μL	588 μL	600 μL
Mono-Methyl-Histone H3 (Lys4)*	55800S	1:50	12 μL	588 μL	600 μL
Di-Methyl-Histone H3 (Lys4)*	31777S	1:50	12 μL	588 μL	600 μL
Tri-Methyl-Histone H3 (Lys4)*	62255S	1:50	12 μL	588 μL	600 μL
Acetyl-Histone H3 (Lys9) **SCC**	28036S	1:50	6 μL	294 μL	300 μL
Acetyl-Histone H3 (Lys27) **SCC**	15562S	1:50	6 μL	294 μL	300 μL
Mono-Methyl-HistoneH3(Lys4)**SCC**	55800S	1:50	6 μL	294 μL	300 μL
Di-Methyl-Histone H3 (Lys4) **SCC**	31777S	1:50	6 μL	294 μL	300 μL
Tri-Methy-Histone (Lys4) **SCC**	62255S	1:50	6 μL	294 μL	300 μL
Histone H3 647 **SCC**	12230S	1:50	6 μL	294 μL	300 μL
Live/Dead **SCC**	L34963	n/a	n/a	n/a	n/a

*** Denotes that the antibody can be combined into their respective sample.**

Background	
Cell line ID	KMT2D10
Gene	KMT2D
Condition	Gene involved in Kabuki Syndrome II
Allele Characteristics	*KMT2D*2del* | -2 indel at 100% | Homozygous KO
Derived from Cell Line	WTC11 | UCSFi001-A
Subclones	KMT2D-3.10.1
	KMT2D-3.10.3
	KMT2D-3.10.4

Genomic Features	
Genomic Coordinates	chr12:49054994
Genomic Sequence	CCCAAG--CCACTGAGTCA
Coordinate,original sequence, change, allele	12,49054994,CCAAGTGCCA,CCAAGCCA,KMT2D102BPDEL

Gene Editing Reagents	
Nuclease	Cas9
sgRNA	sgRNA3 CRISPRevolution sgRNA EZ Kit (1.5 nmol) - KMT2D+49054996
	GGUCUGACUCAGUGGCACUU - Modified
PAM sequence	GGG

DNA Primers for Validation	
PS-KMT2Dex2-F1	GCTGGCTGGTGAGGATAAAG
PS-KMT2Dex2R1	CCGCAGTTACAGAGAGCACA
Sanger Sequencing	Same

Primer	Position	Product Size
Primer PS-KMT2Dex2-F1	+ / 5504	598
PS-KMT2Dex2R1	– / 6063	

Primer Pair Information Edit · Unlink

Link Primers

	Name	T_m
Forward Primer	Primer PS-KMT2Dex2-F1	54.8°C
Reverse Primer	PS-KMT2Dex2R1	56.5°C

Product Size 598 bp
T_m Difference +1.7° C

Supplementary File 2. NxN plots to assess unmixing quality.

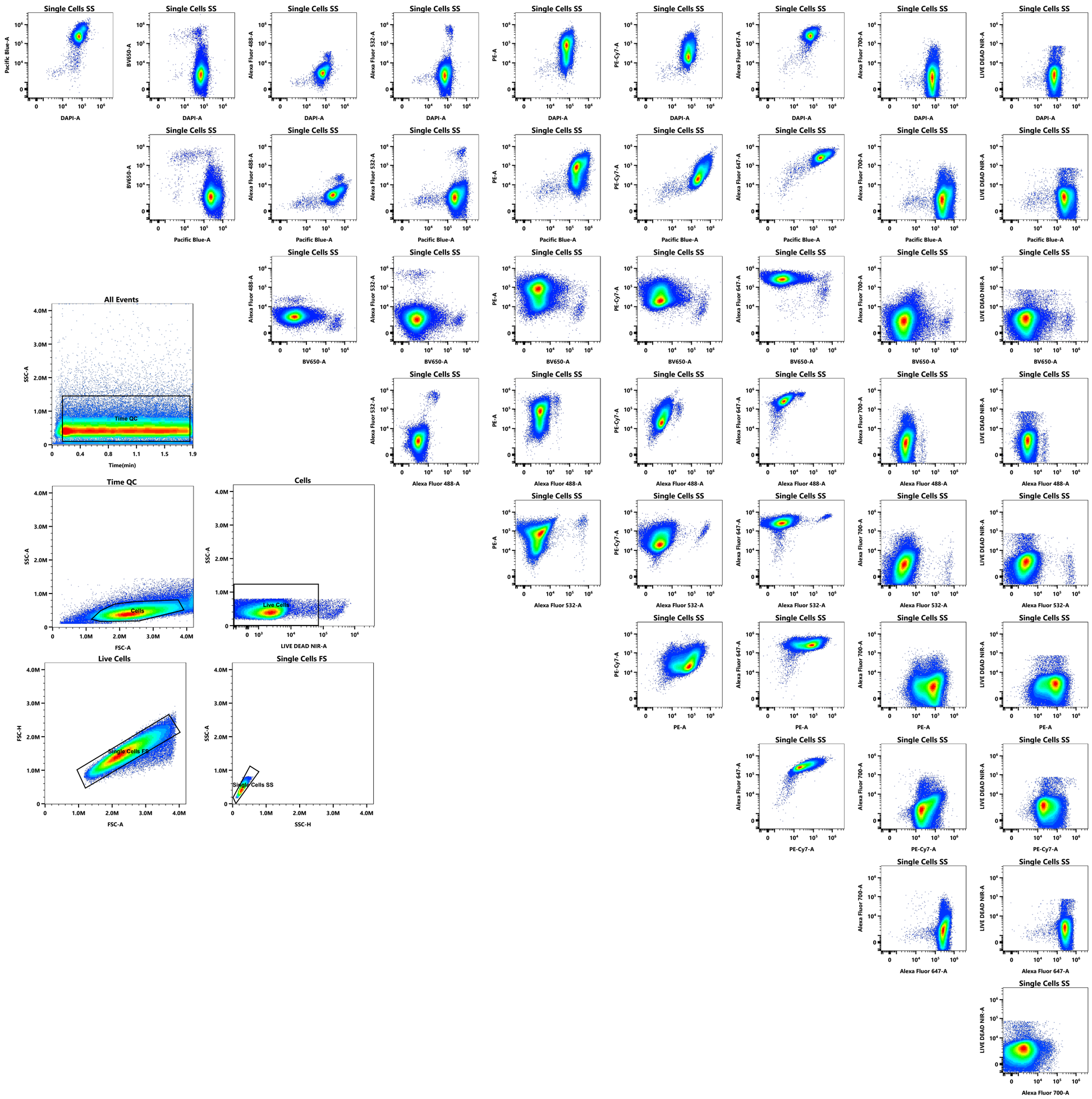

Topic	Strategy	Settings
Compensation	PE-Cy7-A into Alexa Fluor 532-A	-10
Scaling	Arcsinh	co-factor 13000 for Alexa Fluor 700
	Arcsinh	co-factor 6000 for all other features
Gating QC	Time>Singlets>Cells>Live Cells	Fig. 1
Gating H3-PTM	Cleaved caspase-3 + | Apoptotic cells	Fig. 1
	PAX6+ Cells > G0/G1 > H3-PTM	H3K4me3
	PAX6+ Cells> G2 > H3-PTM	H3K9ac
	PAX6+ Cells> phH3 + | Mitotic >H3-PTM	H3K27ac
	PAX6- Cells > G0/G1 > H3-PTM	H3K14ac
	PAX6- Cells> G2 > H3-PTM	were gated as low | Medium | High
	PAX6- Cells> phH3 + | Mitotic >H3-PTM	
Subset Files	Fully stained samples were kept for downstream analysis	
Subsampling	Maximum number of events available in Live Cells Filter	n=97,768 cells avalilable (n=3) | Total cells available in live filter = 61,711
Dimension Reduction	PCA | Features	This was not embedded in downstream opt-SNE
	Violet | FxCycle	Num result components: 2
	Pacific Blue-A | H3K9ac	Method: randomized
	BV650-A | Cleaved-Caspase3	Random seed: 4691
	Alexa Fluor 488-A | H3K14ac	
	Alexa Fluor 532-A | phH3_S10	
	PE-A | PAX6	
	PE-Cy7-A | H3K27ac	
	Alexa Fluor 647-A | H3K4me3	
	Alexa Fluor 700-A | Total H3	
Dimension Reduction	opt-SNE | Features	Fig. 2
	Violet | FxCycle	Max Iterations: 1000
	Pacific Blue-A | H3K9ac	opt-SNE End: 5000
	BV650-A | Cleaved-Caspase3	Perplexity: 50
	Alexa Fluor 488-A | H3K14ac	Theta: 0.5
	Alexa Fluor 532-A | phH3_S10	Components: 2
	PE-A | PAX6	Random seed: 8201
	PE-Cy7-A | H3K27ac	Verbosity: 25
	Alexa Fluor 647-A | H3K4me3	
	Alexa Fluor 700-A | Total H3	
Clustering	FlowSOM | Features	Fig. 2
	Violet | FxCycle	xdim: 9
	Pacific Blue-A | H3K9ac	ydim: 9
	BV650-A | Cleaved-Caspase3	# of training iterations: 15
	Alexa Fluor 488-A | H3K14ac	Distance Metric: euclidean
	Alexa Fluor 532-A | phH3_S10	Kmean: Elbow Metaclustering
	PE-A | PAX6	random seed: 28104
	PE-Cy7-A | H3K27ac	10 fsom clusters. Originally, 11 clusters were generated but cluster 03 was identified as debris and merged with cluster 08 (apoptotic cells). Former cluster 04 was renamed to cluster 03 and so on.
	Alexa Fluor 647-A | H3K4me3	
	Alexa Fluor 700-A | Total H3	
Data export 1	Biological replicates were concatenated and data was exported for fsom gates and manual gates	Scaled per Scaling settings
Data export 2	Clustered Heatmap of Medians was exported for concatenated biological replicates	Row distance: euclidean Row Linkage: ward

Nuclear Histone 3 Post-translational Modification Profiling in Whole Cells using Spectral Flow Cytometry

Histone H3 modification profiling using spectral flow

Carly S Golden[1*], Saylor Williams[1*], Sophia Blankevoort[2], Anna Belkina[1,3], H. Joseph Yost[4], Maria A Serrano[1‡]

[1]Center for Regenerative Medicine, Department of Medicine, Boston University Chobanian & Avedisian School of Medicine, Boston, USA

[2]John and Marcia Price College of Engineering, University of Utah

[3]Flow Cytometry Core Facility, Boston University Chobanian & Avedisian School of Medicine, Boston, USA

[4] The University of Utah, Salt Lake City, Utah and The Catholic University of America, Washington DC, USA

‡ For correspondence: maserr@bu.edu

*Contributed equally to this work

All Figures have been embedded in the main text.